Chapter 4

Preparation of Corrosion-Resistant Films on Magnesium Alloys by Steam Coating

Takahiro Ishizaki, Mika Tsunakawa, Ryota Shiratori, Kae Nakamura and Ai Serizawa

Additional information is available at the end of the chapter

http://dx.doi.org/10.5772/66365

Abstract

This chapter introduces a novel, chemical-free "steam coating" method for preparing films on magnesium (Mg) alloys and assesses their effectiveness in improving the corrosion resistance of two different Mg alloys. A film composed of crystalline $Mg(OH)_2$ and Mg-Al layered double hydroxide (LDH) was successfully formed on AZ31 Mg alloy, and its corrosion resistance was evaluated through electrochemical measurements and immersion tests in an aqueous solution containing 5 wt.% NaCl. An anticorrosive film was also formed on Ca-added flame-resistant AM60 (AMCa602) Mg alloy via the same steam coating method and found to be composed of crystalline $Mg(OH)_2$ and Mg-Al layered double hydroxide (LDH). Its corrosion resistance was also investigated, and the effectiveness of the steam coating method for improving the corrosion resistance of Mg was fully explored.

Keywords: magnesium alloy, steam coating, corrosion resistance, surface treatment, composite film

1. Introduction

Magnesium (Mg) alloys have excellent physical and mechanical properties, including a high specific strength, excellent formability, good vibration adsorption, and high damping capacity [1–5]. However, the greatest advantage of Mg alloys is their lightweight, which has made it possible to achieve energy savings in automobiles, ships, trains, and airplanes through the use of steel-based hybrid materials. In such applications, Mg is superior to aluminum and CFRP (carbon fiber reinforced plastics) in terms of its density and specific strength but offers a much lower corrosion resistance. Various surface treatments have therefore been developed to produce protective coatings on Mg alloys through anodizing, chemical conversion, plasma electrolytic oxidation, or polymer films [6–12].

Chemical conversion has already been used with automotive Mg components because of its ease of operation and low cost, with chromate-based systems the most popular and effective option for producing a protective layer on various metal surfaces [13–15]. The use of chromate, however, is becoming increasingly more regulated due to the high toxicity of hexavalent chromium compounds [16]. Other chemical conversion methods for imparting Mg alloys with a high corrosion resistance have been developed around using tin, rare earth salts, phosphates/permanganates [17–22], vanadium, or composite films of molybdenum-lanthanum or zinc-phosphate-calcium [23, 24].

Films produced by anodizing have also been used to improve the corrosion resistance of Mg alloys, with good results being achieved through the use of micro-arc oxidation (MAO) [25–27]. Using this method, a high anodic voltage (>200 V) is used to locally melt the surface of the Mg alloy and create a ceramic coating [27]. Alkaline electrolytic solutions containing aluminate [28–31], silicate [32–38], or phosphate [39–45] are often used during the MAO of Mg alloys, but the need to treat the liquid waste before disposal creates a risk of environmental pollution due to heavy metal ions. Furthermore, their use may inhibit the recycling of post-use Mg product scraps into Mg ingot. There is therefore a need for an environmentally friendly surface treatment method that is capable of improving the low corrosion resistance of Mg alloys.

A chemical conversion method that creates a protective film of Mg-Al layered double hydroxide (LDH) has recently been used to significantly improve the corrosion resistance of Mg alloys [46–50]. The layered structure of the LDH consists of positively and negatively charged substances with a general molecular formula of $[M_{1-x}^{2+}M_x^{3+}(OH)_2]^{x+}[A_{x/n}^{n-}] \cdot mH_2O$ [51], where M^{2+} and M^{3+} represent divalent and trivalent metal cations, respectively; A^{n-} is an anion such as CO_3^{2-}, SO_4^{2-}, or OH^-; and x has a value of between 0.2 and 0.33 [51]. This structure serves to store and release corrosion inhibitors on demand, thereby creating anion exchange between these inhibitors and chloride ions. This, in turn, results in a self-healing and corrosion-resistant film [52–54]. Tedim et al. reported that LDH nanocontainers loaded with different corrosion inhibitors such as vanadate, phosphate, and 2-mercaptobenzothiazolate (MBT) can improve active corrosion protection [55], with the release of MBT from LDH nanocontainers in a sol-gel film preventing degradation at the metal/film interface. They have also since developed a novel self-healing protective coating using LDH nanocontainers with corrosion inhibitors [56] formed directly on 2024 aluminum alloy via a conversion reaction. Montemor et al. demonstrated that using LDHs loaded with mercaptobenzothiazole in combination with cerium molybdate hollow nanospheres filled with 2-mercaptobenzothiazole results in a synergistic corrosion inhibition effect that has self-healing potential [57].

Though it is clear that LDHs loaded with corrosion inhibitors are effective in substantially improving corrosion resistance, it has also been reported that LDHs devoid of any corrosion inhibitor could also be effective in delaying corrosion by trapping anions such as chloride ions in LDHs [58, 59]. Lin et al., for example, have shown that the CO_3^{2-} in carbonate Mg-Al LDH has Cl^- anion-exchangeability in a corrosive environment and so can protect Mg alloy against corrosion [58]. Tedim et al. have also reported that Cl^- ions in a corrosive environment can

http://dx.doi.org/10.5772/66365

be trapped in the interlayer of Zn-Al LDH intercalated with nitrate anions and that the addition of this LDH to a polymer layer drastically reduces the permeability of corrosive Cl^- ions through the protective coating. This confirms that LDHs are a promising material for improving corrosion resistance [59], but anticorrosive films containing LDHs are usually prepared by a multistep process in which LDHs are first synthesized in powder form and then incorporated into a film for corrosion protection [53]. For industrial applications, it is important to develop an environmentally friendly surface treatment method for achieving an anticorrosive film containing LDHs in a single step.

This chapter presents experimental results pertaining to the preparation and corrosion resistance of magnesium hydroxide films containing Mg-Al LDH on two types of Mg alloy: AZ31 and a flame-resistant Ca-added AM60 (AMCa602). A comparison is also made of the corrosion potentials and corrosion current densities obtained by polarization curve measurements in 3.5 mass% NaCl aqueous solution of films prepared on AZ31 alloy by various methods such as physical vapor deposition, chemical vapor deposition, anodization, chemical conversion, plasma electrolytic oxidization (PEO), spin coating, and a newly developed steam coating method for producing a hydroxide film containing Mg-Al LDH [10–12, 23, 24, 60–65]. As shown in **Table 1**, steam coating produces a relatively positive corrosion potential and the lowest corrosion current density of all the films tested, which indicates that this method imparts superior corrosion resistance. Furthermore, the direct growth of such films from the Mg alloy itself can greatly improve their adherence and mechanical stability when compared to other methods such as spin coating and dip coating [66].

Treatment method	Main component in each film	Corrosion potential (V vs. Ag/AgCl)	Corrosion current density (A/cm^2)	Ref.
PVD	Al_2O_3	−1.51	9.20×10^{-5}	[60]
PVD	TiO_2	−1.50	1.29×10^{-4}	[61]
CVD	SiOx	−1.37	1.58×10^{-7}	[62]
CVD	SiOx	−1.59	4.3×10^{-7}	[63]
Anodization	Mg-Al LDH + MgO	−1.19	3.82×10^{-7}	[10]
Chemical conversion	$MgO + Mg_2SiO_4 + Al_2O_3$	−0.06	9.47×10^{-6}	[12]
Chemical conversion	Vanadium	−1.05	8.60×10^{-6}	[23]
Chemical conversion	Mo/La	−1.54	1.15×10^{-7}	[24]
PEO	$Zn_3(PO_4)_2$	−1.76	1.04×10^{-7}	[60]
PEO	$MgO + Mg_3(PO_4)_2$	−1.50	4.00×10^{-8}	[64]
PEO	$Mg_2SiO_4 + CeO_2$	−1.20	2.00×10^{-8}	[65]
Spin coating	$TiO_2 + MgAl_2O_4$	−1.26	4.90×10^{-6}	[74]

PVD, plasma vapor deposition; CVD, chemical vapor deposition; PEO, plasma electrolytic oxidation.

Table 1. Corrosion potentials and corrosion current densities obtained by polarization curve measurements in 3.5 mass% NaCl aqueous solution for films prepared by various methods.

2. Preparation of Mg-Al layered double hydroxide films on AZ31 Mg alloy

In this section, we introduce a method for preparing a protective magnesium hydroxide film containing Mg-Al LDH on specimens of AZ31Mg alloy (composition: 2.98% Al, 0.88% Zn, 0.38% Mn, 0.0135% Si, 0.001% Cu, 0.002% Ni, 0.0027% Fe, remainder Mg) measuring 20 × 20 × 1.5 mm. These AZ31 substrates were prepared by ultrasonically cleaning them in absolute ethanol for 10 min and then drying with inert Ar gas. Once clean, the substrates were set on a substrate stage in a 100 ml-capacity, Teflon-lined autoclave, which had 20 mL of ultrapure (resistance of 18.2 MΩ cm) located at the bottom to produce steam. The distance between the water surface and substrate stage was c.a. 3 cm. The autoclave was heated to a temperature of 423–453 K and then held at this temperature for 1–8 h before being allowed to cool naturally to room temperature. After this steam coating treatment, the samples were ultrasonically cleaned in ethanol for 10 min and dried with Ar gas.

The appearance of the samples after steam coating (**Figure 1**) reveals that all the substrates treated at 423–443 K were uniformly covered with film, regardless of the treatment time. However, as partial detachment of the film was observed in the case of the substrates treated at 433 K for 8 h and at 453 K for 3 and 4 h, these treatment conditions are not considered suitable for preparing an anticorrosive film. The detachment of the film was also found to become more prominent with an increase in the treatment time.

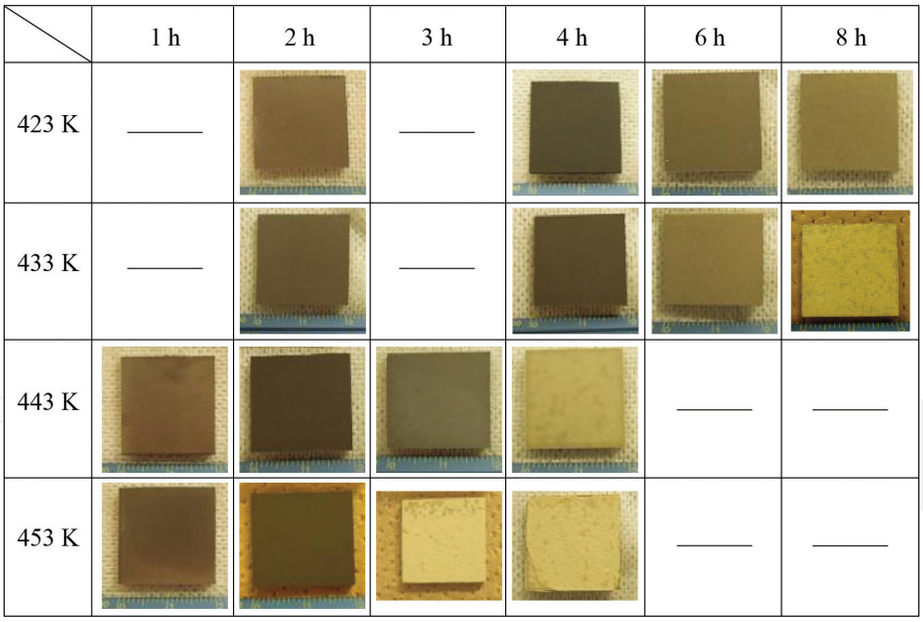

Figure 1. Digital photographs showing the surface of 2 × 2 cm-sized samples prepared under different conditions of temperature and duration [reproduced by permission of the Royal Society of Chemistry, Journal of Materials Chemistry A, 2013, 1, 8968–8977].

The GAXRD patterns of the films formed on AZ31 with different treatment times (423, 433, 443, and 453 K) shown in **Figure 2** reveal clear peaks attributable to the Mg alloy substrate at treatment times less than 2 h with all treatment temperatures. An additional peak at around

http://dx.doi.org/10.5772/66365

2θ = 18° assigned to the 0 0 1 diffraction peak of brucite-type $Mg(OH)_2$ is present in samples treated at 423 and 433 K for 2 h and at 443 and 453 K for 1 h. A diffraction peak consistent with [1 0 1] reflection at around 2θ = 38°, which has the highest intensity according to the JCPDS file number 44-1482, becomes stronger with increasing treatment time at all treatment temperatures, which suggests the formation of hexagonal $Mg(OH)_2$. With an increase in treatment time, several reflection lines at 2θ angles of approximately 18, 33, 38, 51, 58, 62, 68, and 72° are clearly observed in all the GAXRD patterns, and these can be assigned to the 0 0 1, 1 0 0, 1 0 1, 1 0 2, 1 1 0, 1 1 1, 2 0 0, and 2 0 1 reflections of brucite-type $Mg(OH)_2$, respectively. When the treatment time is increased to more than 3 h at any of the treatment temperatures, then one or two peaks attributable to a hydrotalcite (HT)-like structure are also observed. These are attributed to the formation of $Mg_{1-x}Al_x(OH)_2(CO_3)_{x/2}{\cdot}nH_2O$ (Mg-Al LDH) intercalated with carbonate anions. The two peaks at 2θ angles of around 11° and 22° were assigned to the [0 0 3] and [0 0 6] reflections of $Mg_{1-x}Al_x(OH)_2(CO_3)_{x/2}{\cdot}nH_2O$, respectively (JCPDS No. 41-1428). Based on these XRD results, it is concluded that the most suitable treatment conditions for preparing a film composed of $Mg(OH)_2$ and Mg-Al LDH are 423 K for 6–8 h, 433 K for 4–6 h, 443 K for 3–4 h, and 453 K for 2 h.

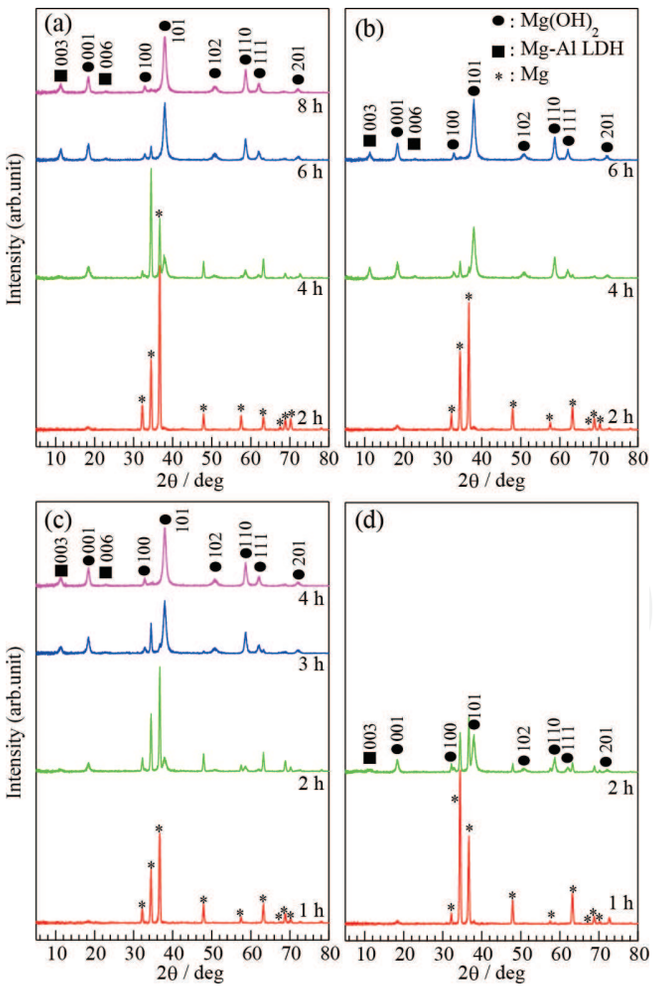

Figure 2. XRD patterns of samples treated at (a) 423 K, (b) 433 K, (c) 443 K, and (d) 453 K [reproduced by permission of the Royal Society of Chemistry, Journal of Materials Chemistry A, 2013, 1, 8968–8977].

The most dominant feature of the FT-IR spectra of the samples treated at 423, 433, 443, and 453 K in **Figure 3** is an intense sharp peak at 3696.9 cm^{-1}. It has been reported that pure $Mg(OH)_2$ exhibits a single band at 3698 cm^{-1} due to the high basicity of its O—H groups [67], and this peak was clearly presented in those samples treated at 423 K for more than 4 h, 433 K for 2–6 h, 443 K for over 2 h, and 453 K for 2 h. These results are in agreement well with their respective XRD profiles. The peak and shoulder bands observed at 950, 781, and 558 cm^{-1} can be attributed to Al—OH translation modes [68], while the bands at 1370–1520 cm^{-1} are attributed to symmetric and asymmetric stretching modes of CO_3^{2-} in the interlayer [68, 69]. These peaks and bands could only be detected in the spectra of samples which exhibited peaks attributable to Mg-Al LDH in their XRD pattern. An additional band at 1630–1650 cm^{-1} was assigned to the bending mode of water molecules in the interlayer. A shoulder band at 3080 cm^{-1} revealed the presence of hydrogen bonding between water and CO_3^{2-} in the interlayer [68]. These results indicate that the films treated at 423 K for more than 4 h; at 433 K for 2, 4, and 6 h; at 443 K for more than 2 h; and at 453 K for 2 h were composed of crystalline $Mg(OH)_2$ and carbonate Mg-Al LDH.

The SEM images in **Figure 4** show the surfaces of samples treated at 433 K, in which we see that steam coating for 2 h led to a rougher and more nodular surface than the untreated AZ31. Several pores of up to several hundred nanometers in diameter were also observed on the surface. When the preparation time was prolonged to 4 h, granular structures were formed and the film was found to be denser than after 2 h. However, a number of pores measuring several hundred nanometers in diameter were still observed on the surface. With the sample treated for 6 h, the film was found to be denser than after 4 h of treatment, with no pores evident on the surface.

Figure 5 presents SEM images showing the sample surfaces treated at 443 K. Note that when the deposition time was less than 1 h, there was only a very low localized surface coverage of the film. However, the surface became fully covered with film when the treatment time was extended to more than 2 h, and this coverage became denser with increasing treatment time. As such, the sample treated for 4 h had a denser film than the sample treated for 3 h, which means that surface topography could be effective way of improving the corrosion resistance.

Figure 6 shows a cross-sectional SEM image and EDX spectrum of the sample treated at 443 K for 4 h, as well as elemental mapping images for Mg, O, and Al. As shown in **Figure 6(a)**, the film produced on this sample had a thickness of about 52 μm, whereas treatment at 423 K for 4 and 6 h, at 433 K for 4 and 6 h, at 443 K for 3 h, and at 453 K for 2 h produced film thicknesses of about 5, 35, 20, 68, 19, and 7 μm, respectively, based on their cross-sectional SEM images. The elemental mapping images in **Figure 6(b)** revealed that the film mainly consisted of Mg and O, which indicates that it was comprised of magnesium hydroxide. This is in agreement well with the XRD results and FT-IR spectrum for the sample. A trace amount of Al was also detected, which provides evidence that Mg-Al LDH exists slightly and locally in the film. The XRD, FT-IR, and SEM-EDX results reveal that steam coating method can produce Mg-Al LDH in the resulting surface film.

Based on these results presented thus far, a model for the formation of the film is proposed as follows. In the closed reaction vessel, steam is produced from water by thermal energy until the vessel becomes saturated. The high pressure and temperature mean that this water vapor has a high kinetic energy and reactivity, which leads to the dissolution of Mg and Al metal into Mg^{2+} and Al^{3+} ions. It is considered likely that $Mg(OH)_2$ crystallites grow via a dissolu-

http://dx.doi.org/10.5772/66365

tion-precipitation mechanism, as Nordlien et al. have suggested that amorphous platelets of $Mg(OH)_2$ are initially formed by the precipitation of Mg^{2+} or other soluble Mg species [70]. In addition, Mg^{2+} and Al^{3+} ions might react with the steam to form carbonate Mg-Al LDH, with carbonate ions being sourced from CO_2 present in the enclosed autoclave atmosphere prior to steam treatment. The water vapor can also penetrate the composite film due to the difference in pressure and its high kinetic energy, where it can then react with the Mg alloy substrate.

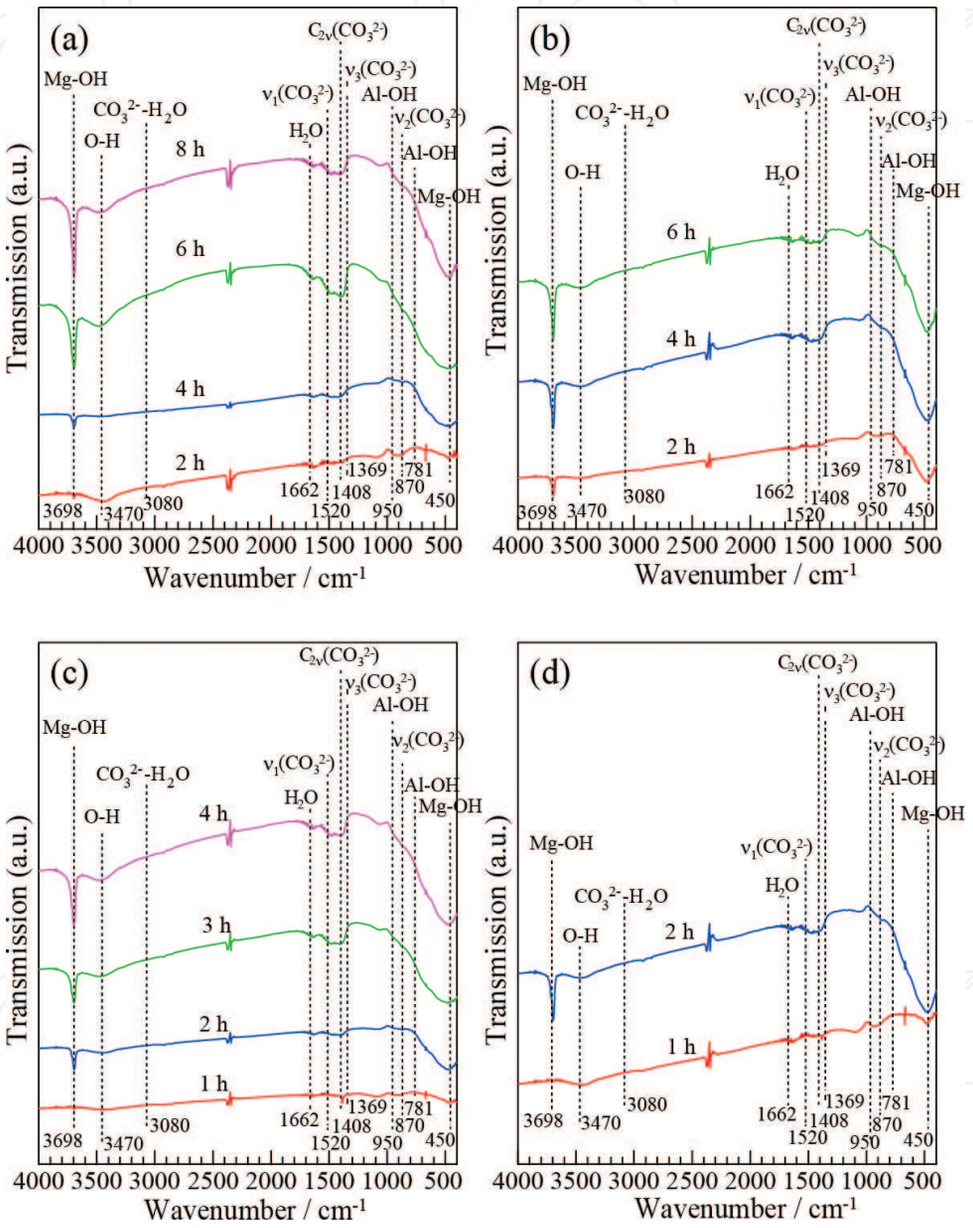

Figure 3. FT-IR spectra of samples treated at (a) 423 K, (b) 433 K, (c) 443 K, and (d) 453 K [reproduced by permission of the Royal Society of Chemistry, Journal of Materials Chemistry A, 2013, 1, 8968–8977].

As a result, a film composed of magnesium oxide/hydroxide and carbonate Mg-Al LDH is prepared directly on the AZ31 substrate. This direct growth of a film from a substrate is a strong advantage over other methods, as this can greatly improve the mechanical stability and adherence of the film. It has also been reported that the existence of Mg-Al LDH in a film

prevents metals such as Al and Mg from occurring the corrosion reaction, and so the films produced here are expected to provide a high corrosion resistance.

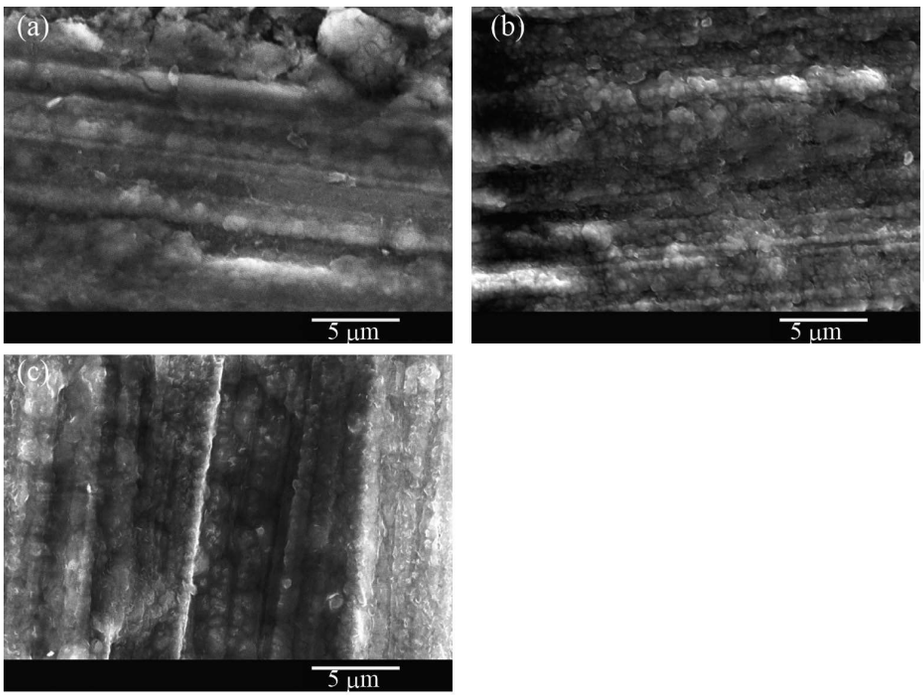

Figure 4. SEM images of samples treated at 433 K for (a) 2, (b) 4, and (c) 6 h [reproduced by permission of the Royal Society of Chemistry, Journal of Materials Chemistry A, 2013, 1, 8968–8977].

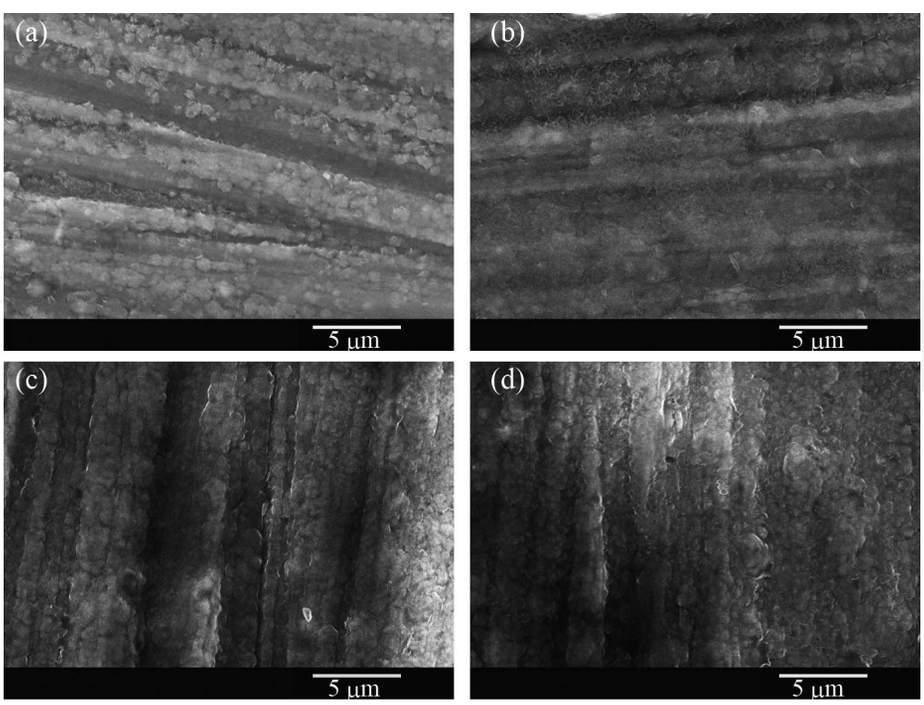

Figure 5. SEM images of samples treated at 443 K for (a) 1, (b) 2, (c) 3, and (d) 4 h [reproduced by permission of the Royal Society of Chemistry, Journal of Materials Chemistry A, 2013, 1, 8968–8977].

http://dx.doi.org/10.5772/66365

The corrosion resistance of the films formed on AZ31 Mg alloy was investigated via potentiodynamic polarization curve measurements, i.e., the lower the polarization current, the better the corrosion resistance. **Figure 7** shows the potentiodynamic polarization curves for the samples treated at 423, 433, 443, and 453 K and untreated AZ31. The corrosion potentials (E_{corr}) and corrosion current densities (i_{corr}) for samples treated under different conditions are listed in **Table 2**. The E_{corr} and i_{corr} values for the bare AZ31 were estimated to be ca. −1.43 V vs. Ag/AgCl and 5.39×10^{-5} A/cm^2, respectively. The anodic region of the curve for the bare AZ31 can be divided into three fields: (i) first region beginning from E_{corr} (low anodic over potential) that exhibits a linear increase in current density with potential; (ii) a range of abrupt increase in current density from −1.4 V, where the dissolution of Mg to Mg^+ or Mg^{2+} ions predominantly occurred [71]; and (iii) a current plateau at more positive potentials, where the electrode surface is covered with a film identified as $Mg(OH)_2$ [72]. In the cathodic branch, hydrogen evolution is more dominant at negative potentials than E_{corr}, resulting in an increase in the cathodic current density. The current densities of the anodic and cathodic branches of all samples decreased with film formation, which indicates that the films are effective in improving the corrosion resistance of AZ31 alloy.

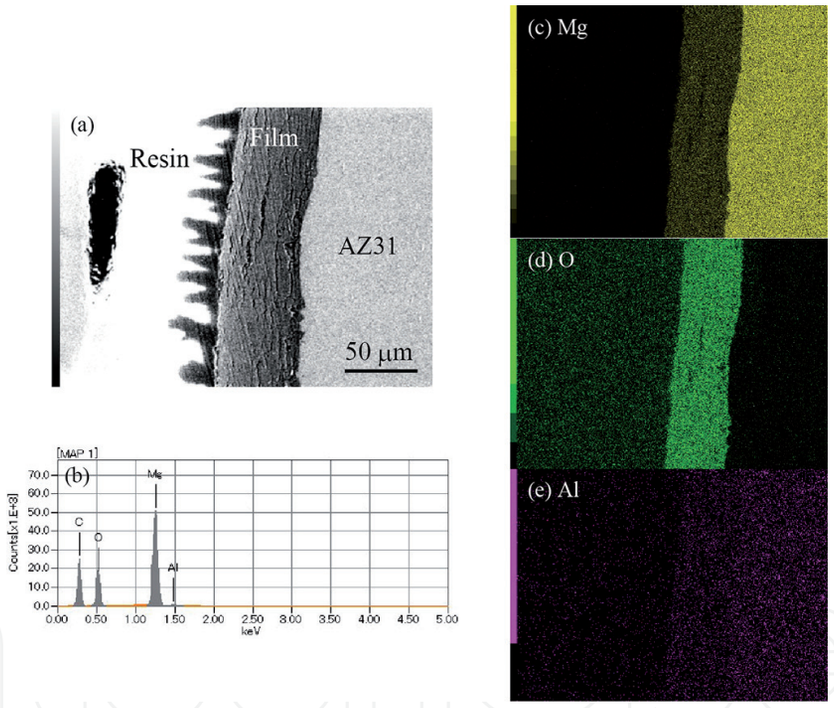

Figure 6. (a) Cross-sectional SEM image of the sample treated at 443 K for 4 h and (b) the corresponding EDX spectra. (c) Elemental maps for (c) Mg, (d) O, and (e) Al [reproduced by permission of the Royal Society of Chemistry, Journal of Materials Chemistry A, 2013, 1, 8968–8977].

At all treatment temperatures, the E_{corr} tends to shift in a positive direction with increasing process time. Furthermore, at potentials more positive than E_{corr}, clear passive ranges can be presented in the curves of the samples treated at 423 K for over 6 h, at 433 K for more than 4 h, at 443 K for more than 2 h, and at 453 K for 2 h. This existence of a long passive range means that the film coatings on AZ31 exhibit highly corrosive-resistant properties in solutions containing Cl^- ions. An abrupt increase in current density at more positive potentials than E_{corr}

could be seen in the polarization curves of the samples prepared at 423 K for more than 6 h, at 433 K for 4 h, at 443 K for more than 2 h, and at 453 K for 2 h. For example, the samples treated at 423 K for more than 6 h show an increase in current density at approximately −0.7 and 0.3 V, respectively. This increase of current density could be ascribed to pitting corrosion, which would imply that the electrolytic solution permeated through the film due to the presence of cracks or pores. Similar behavior has been reported before, even in aluminum alloys [73]. However, there was no evidence of pitting corrosion in the curve of the sample treated at 433 K for 6 h, which had E_{corr} and i_{corr} values estimated to be −0.161 V and 4.824×10^{-11} A/cm^2, respectively (**Table 2**). These values represent the most positive potential and lowest current density of all the samples, indicating that these conditions produced the best corrosion resistance. We therefore subsequently investigated the durability of the corrosion resistance of a sample treated at 433 K for 6 h when immersed in a 5 wt.% aqueous NaCl solution.

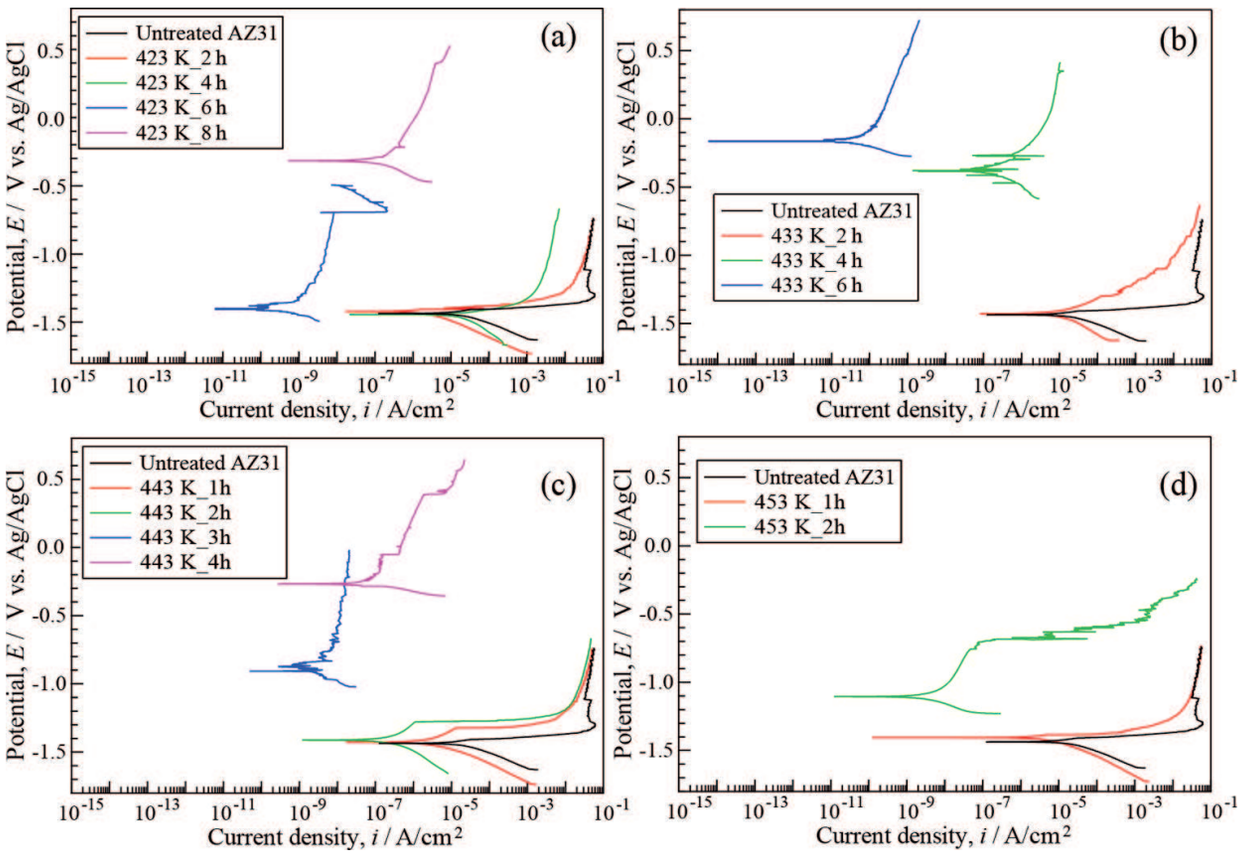

Figure 7. Polarization curves of samples prepared at (a) 423 K, (b) 433 K, (c) 443 K, and (d) 453 K. Polarization curve of bare Mg alloy is also exhibited in respective figure. The scanning rate for all measurements was 0.5 mV/s [reproduced by permission of the Royal Society of Chemistry, Journal of Materials Chemistry A, 2013, 1, 8968–8977].

Figure 8(a) shows the XRD patterns of samples treated at 433 K for 6 h before (black line) and after (dashed red line) immersion in 5 wt.% aqueous NaCl solution for 240 h. The only clear difference in peak intensity is attributable to 0 0 1 reflection of the $Mg(OH)_2$ crystallite, which is much stronger after immersion. This indicates that immersion in a 5 wt.% NaCl solution changes the orientation of the film. The SEM images in **Figure 8**(**b** and **c**) show this change in

http://dx.doi.org/10.5772/66365

the orientation of the $Mg(OH)_2$ film, with immersion making the film aligned at fairly steeply inclined angles with respect to the surface.

Temp.		1 h	2 h	3 h	4 h	6 h	8 h
423 K	E_{corr} V vs. Ag/AgCl	–	−1.427	–	−1.446	−1.389	−0.316
	i_{corr} A/cm^2	–	1.23×10^{-5}	–	3.22×10^{-5}	5.29×10^{-5}	1.29×10^{-7}
433 K	E_{corr} V vs. Ag/AgCl	–	−1.425	–	−0.376	−0.161	–
	i_{corr} A/cm^2	–	1.28×10^{-5}	–	1.79×10^{-7}	4.82×10^{-11}	–
443 K	E_{corr} V vs. Ag/AgCl	−1.427	−1.421	−0.899	−0.265	–	–
	i_{corr} A/cm^2	3.33×10^{-6}	2.48×10^{-7}	1.90×10^{-9}	9.84×10^{-8}	–	–
453 K	E_{corr} V vs. Ag/AgCl	−1.405	−1.104	–	–	–	–
	i_{corr} A/cm^2	1.21×10^{-5}	7.71×10^{-9}	–	–	–	–

Table 2. Fitting results for potentiodynamic curves in 5.0 wt.% NaCl solution of films formed by steam coating at different temperatures.

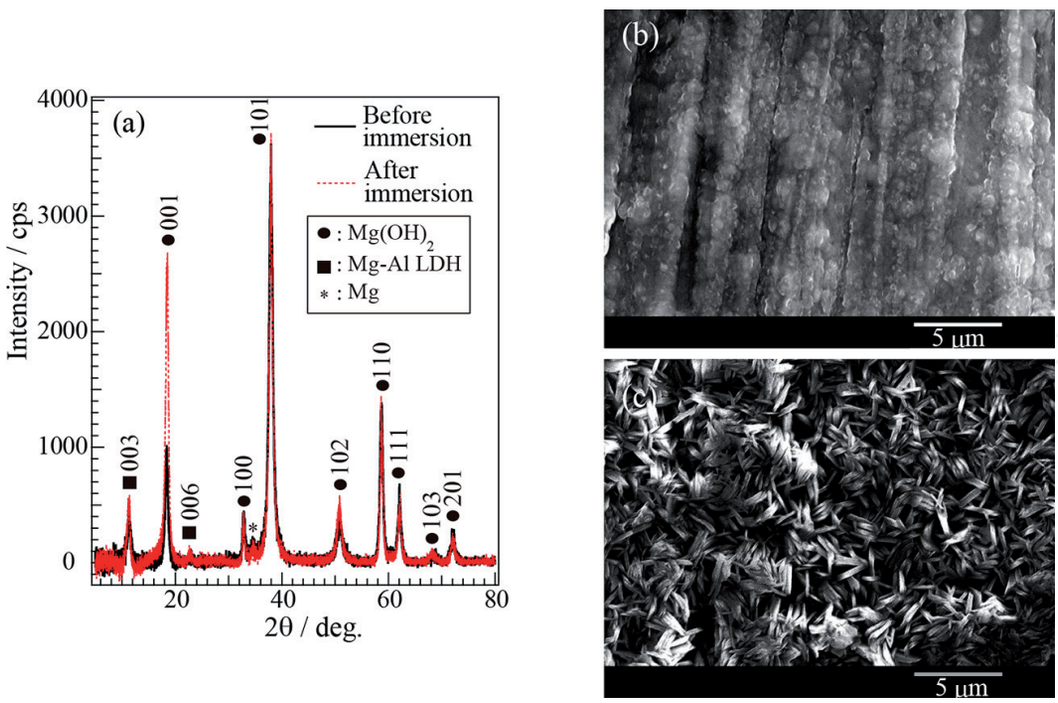

Figure 8. (a) XRD profile of the sample prepared at 433 K for 6 h before and after immersion in 5 wt.% NaCl aqueous solution for 240 h. SEM images of film-coated AZ31 (b) before and (c) after immersion in 5 wt.% NaCl aqueous solution for 240 h [reproduced by permission of the Royal Society of Chemistry, Journal of Materials Chemistry A, 2013, 1, 8968–8977].

The SEM images in **Figure 9** show the sample treated at 433 K for 6 h before and after its immersion in 5 wt.% NaCl solution for 240 h. The visible appearance of these samples is shown in the inset images and reveals that although no physical damage occurred as a result of immersion, there was a slight change in the color of the film. The SEM images show that there was a slight microscale change following immersion, with submicron pores being formed on the surface. A morphological change in the film surface was also observed, with small amounts of nanosheets becoming aligned at fairly inclined angles relative to the surface. This nanosheet formation is in agreement with the XRD patterns and is likely the result of dissolution caused by the film being in contact with the NaCl solution. **Figure 9(c)** presents potentiodynamic polarization curves for the sample treated at 433 K for 6 h before and after immersion in 5 wt.% NaCl solution for 240 h. From this, we see that the E_{corr} after immersion was approximately −0.65 V, which represents a considerable negative shift due to the change in the physicochemical properties of the film. The i_{corr} value, on the other hand, was almost the same before and after immersion. A clear passive region at c.a. 650 mV was observed after immersion, and though there was a slight variation in the current density, this indicates that the film exhibits high corrosion resistance even when immersed in a 5 wt.% NaCl solution for 240 h, as shown by the SEM image in **Figure 10(a)**.

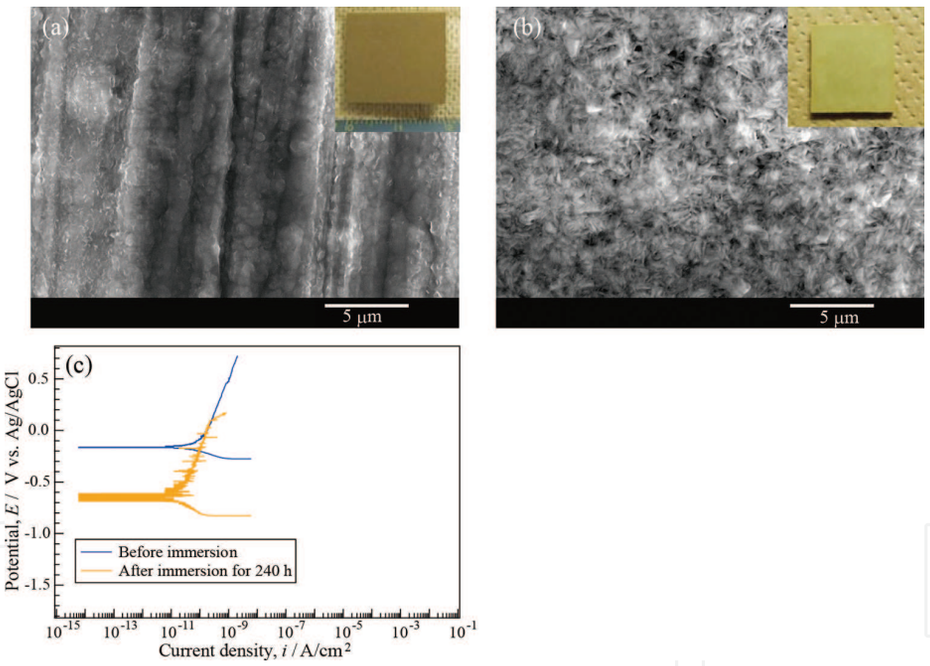

Figure 9. SEM images of the sample prepared at 433 K for 6 h (a) before and (b) after immersion in 5 wt.% NaCl aqueous solution for 240 h. (a) and (b) are photographs showing the appearance of the sample surface. (c) Polarization curves of the sample prepared at 433 K for 6 h before and after immersion in 5 wt.% NaCl aqueous solution for 240 h [reproduced by permission of the Royal Society of Chemistry, Journal of Materials Chemistry A, 2013, 1, 8968–8977].

Figure 10(b–e) shows the EDX spectra obtained at spots (i), (ii), (iii), and (iv) in **Figure 10(a)**. At spots (i) and (ii), there are two peaks attributable to Cl and Al but no peak for Na, whereas no Cl was detected at spots (iii) and (iv). The presence of Al at spots (iii) and (iv) indicates that the Mg-Al LDH layer was still present, which suggests that CO_3^{2-} ions in the Mg-Al LDH

layer were partially exchanged for Cl^- anions. From the XRD patterns and EDX spectra, it is evident that Mg-Al LDH is able to trap some Cl^- ions within its structure, which has been reported to delay the degradation of protective coatings [59]. It is also apparent that carbonate Mg-Al LDH has a weak anion exchangeability. This is significant given that Williams et al. have found LDHs loaded with carbonate and nitrates are more effective than a blank coating in preventing the corrosion of a metallic substrate during filiform corrosion tests [74].

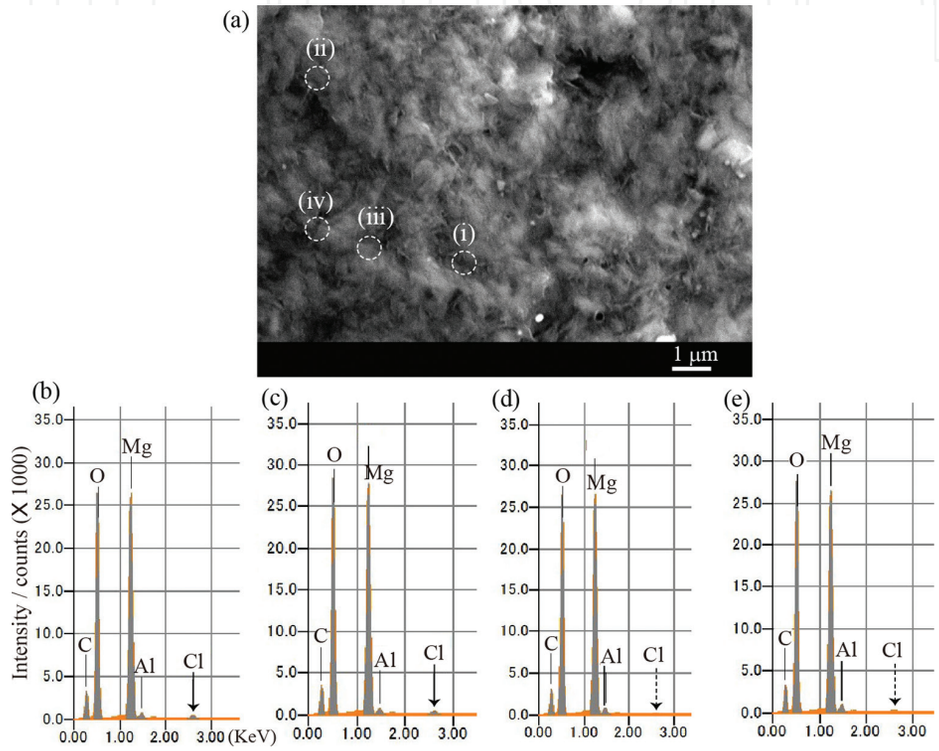

Figure 10. SEM image of the sample treated at 433 K for 6 h after immersion in 5 wt.% NaCl aqueous solution for 240 h. (b), (c), (d), and (e) show EDX spectra obtained at spots (i), (ii), (iii), and (iv) in **Figure 9** (a), respectively [reproduced by permission of the Royal Society of Chemistry, Journal of Materials Chemistry A, 2013, 1, 8968–8977].

This section has shown that a protective magnesium hydroxide film containing Mg-Al layered double hydroxide (LDH) can be produced on Mg alloy via a simple, environmentally friendly, inexpensive, and chemical-free steam coating method. Subsequent XRD and FT-IR studies revealed that these films are composed of $Mg(OH)_2$ and carbonate Mg-Al LDH, and a formation mechanism was proposed based on the results of XRD, FT-IR, SEM, and EDX measurements. Potentiodynamic measurements and immersion tests in 5 wt.% NaCl aqueous solution revealed that a film prepared on AZ31 alloy at 433 K for 6 h provides the greatest corrosion resistance. Increasing the immersion time induced a change in the orientation of the crystalline $Mg(OH)_2$ structure, but no change was observed in the appearance of the sample. With a growing demand for Mg alloys and an increasing focus on environmental issues, it is believed that this steam coating method can provide an effective means of improving the corrosion performance of large, complex-shape Mg alloy components.

3. Formation of Mg-Al layered double hydroxide films on flame-resistant AM60 Mg alloy

In the previous section, we characterized the properties of an anticorrosive film composed of $Mg(OH)_2$ and Mg-Al LDH that is formed on commercial AZ31 Mg alloy by steam coating. In this section, we report on the formation and properties of the anticorrosive film that is produced in a similar manner on Ca-added AM60 Mg alloy (AMCa602), which is one of the most important lightweight materials for transportation components because of its flame-resistant nature. This unique trait is the result of the fact that Ca will oxide before Mg ignites [75], which increases the ignition temperature from 200 to 300 K and greatly restrains the inherently combustible nature of Mg alloys. However, as this addition of Ca does not improve the low corrosion resistance of Mg alloy, there is still a need to develop a suitable surface treatment technology.

Although anodized, chemical conversion and polymer films have all been applied to Mg alloys [6–9, 76–81], there have been few reports pertaining to the surface treatment method of flame-resistant Mg alloys. Xia et al. did find that the corrosion resistance of Mg-4.0Zn-0.2Ca alloy is improved by micro-arc oxidization (MAO) treatment in basic aqueous solutions containing Na_4SiO_4, NaF, and NaOH due to the formation of a film composed mainly of MgO and MgF_2 [82]; however, the presence of fluorine atoms in such coatings creates a risk of environmental pollution. Mori et al. reported on the preparation and corrosion resistance of a plasma electrolytic oxidation layer on nonflammable Ma-Al-Mn-Ca Mg alloy (AMCa602), which was mainly composed of Mg_2SiO_4 and MgO [83]. The liquid waste produced during this anodization process, however, needs to be treated prior to disposal. There is therefore still a need for an environmentally friendly surface treatment capable of improving the low corrosion resistance of flame-resistant Mg alloys.

Specimens of AMCa602 Mg alloy (composition in wt.%: 5.92% Al, 0.36% Mn, 1.99% Ca, <0.01% Si, <0.01% Cu, <0.005% Ni, <0.005% Fe, balance Mg) measuring 20 × 20 × 1.5 mm in size were supplied by Fuji Light Metal Co., Ltd. These Mg alloy substrates were ultrasonically cleaned in absolute ethanol for 10 min and then dried with inert Ar gas. Once clean, they were placed on a substrate stage in a Teflon-lined, 100 ml-capacity autoclave, into which 20 mL of ultrapure water containing 0, 2, 20, or 200 mM $Al(NO_3)_3 \cdot 9H_2O$ was added to the bottom to produce steam. The distance between the surface of the water and the substrate stage was around 3 cm. The autoclave was heated to a temperature of 433 K, where it was held for 6 h before being allowed to cool naturally to room temperature. Following this steam treatment, the samples were ultrasonically cleaned in ethanol for 10 min and dried with Ar gas.

Figure 11 shows the GAXRD patterns of the films formed on AMCa602 at 433 K over a 6 h period from aqueous solutions containing 0, 2, 20, or 200 mM of $Al(NO_3)_3 \cdot 9H_2O$ in 20 mL of ultrapure water. A weak peak attributable to the Mg alloy substrate is visible at a 2θ angle of approximately 34° in all the patterns. A diffraction peak corresponding to 1 0 1 reflection at approximately $2\theta = 38°$, which has the highest intensity according to JCPDS No. 44-1482, appears slightly weaker with an increase in the $Al(NO_3)_3$ concentration. In addition, several peaks were observed in all the GAXRD patterns at 2θ angles of approximately 18, 33, 51, 58, 62, 68, and 72°

http://dx.doi.org/10.5772/66365

that can be attributed to the 0 0 1, 1 0 0, 1 0 2, 1 1 0, 1 1 1, 2 0 0, and 2 0 1 diffraction peaks of brucite-type $Mg(OH)_2$, indicating the formation of hexagonal $Mg(OH)_2$. In addition to these peaks, one or two peaks attributable to a hydrotalcite (HT)-like structure can be distinguished that are assigned to $Mg_{1-x}Al_x(OH)_2(NO_3)_x{\cdot}nH_2O$ intercalated with nitrate anions [84]. These diffraction peaks are indexed according to 3*R* symmetry, and so the two peaks at around $2\theta = 11°$ and 22° are attributed to the 0 0 3 and 0 0 6 reflections, respectively, of $Mg_{1-x}Al_x(OH)_2(NO_3)_x{\cdot}nH_2O$ [51, 85, 86]. This suggests that the treated surfaces were crystallized with a preferential hexagonal orientation along the (0 0 3) plane, which is a characteristic feature of the spontaneous texture axis of $Mg_{1-x}Al_x(OH)_2(NO_3)_x{\cdot}nH_2O$. Furthermore, these XRD profiles reveal that all films were composed of crystalline Mg-Al LDH and $Mg(OH)_2$, regardless of the $Al(NO_3)_3$ concentration used.

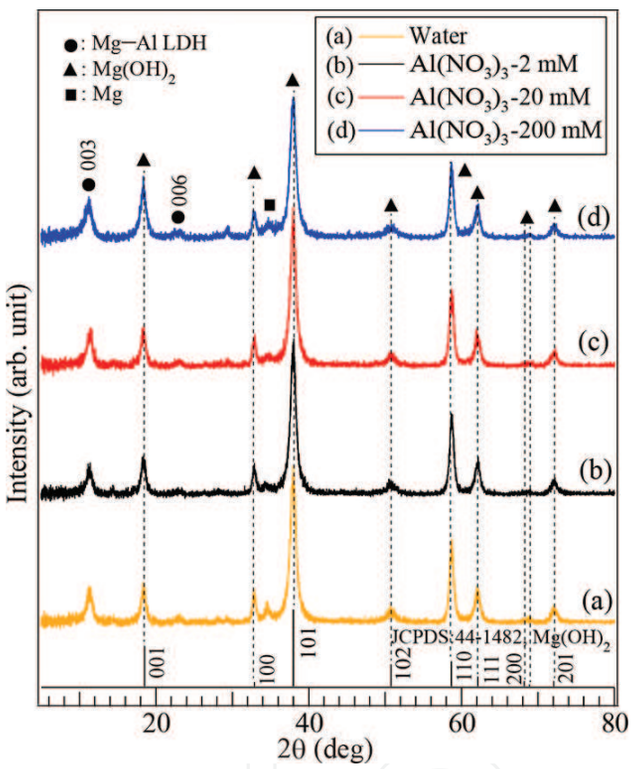

Figure 11. GAXRD patterns of films formed on AMCa602 at 433 K for 6 h from aqueous solutions with $Al(NO_3)_3$ concentrations of (a) 0, (b) 2, (c) 20, and (d) 200 mM [Corrosion Science, 2015, 92, 76–84, doi:10.1016/j.corsci.2014.11.031. Copyright @ELSEVIER (2015)].

The appearances of the samples after steam coating at 433 K for 6 h using aqueous solutions containing $Al(NO_3)_3$ at concentrations of 2, 20, and 200 mM are shown in **Figure 12(a–c)**. Note that in all cases the substrate were uniformly covered with film, but the color of this film did change with $Al(NO_3)_3$ concentration. The SEM images in **Figure 12(d–f)** show the same samples, from which we see that an aqueous solution containing 2 mM $Al(NO_3)_3$ produces a relatively smooth surface with only a few minute pores measuring several hundred nanometers in diameter. The surface of the sample prepared using an aqueous solution containing 20 mM $Al(NO_3)_3$, on the other hand, was quite rough and had a small number of nanosheets that were slightly inclined with respect to the surface.

As shown in **Figure 13**, elemental mapping by EDX revealed traces of elemental Mg, Al, and O primarily in areas where nanosheets existed, which is consistent with the presence of Mg-Al LDH. Aggregated particles are also clearly discernible in these images, which likely formed during steam treatment and condensed on the substrate, and it is on these particles that the nanosheets formed. The sample prepared from an aqueous solution containing 200 mM

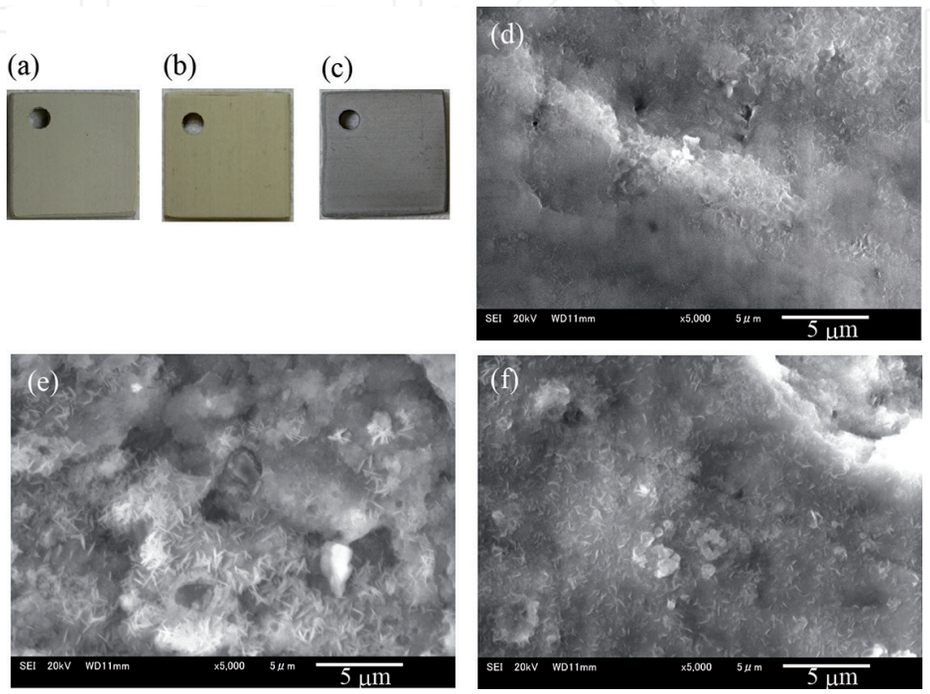

Figure 12. Appearance of samples after steam coating at 433 K for 6 h using aqueous solutions containing $Al(NO_3)_3$ at concentrations of (a) 2, (b) 20, and (c) 200 mM. (d–f) SEM images of the samples shown in (a–c) [Corrosion Science, 2015, 92, 76–84, doi:10.1016/j.corsci.2014.11.031. Copyright @ELSEVIER (2015)].

$Al(NO_3)_3$ was smooth and dense compared to that produced from a 20 mM $Al(NO_3)_3$ solution, and although small nanosheets were formed that were slightly inclined with respect to the surface, no cracks were found in the film.

Figure 14 shows the FT-IR spectra of samples steam coated at 433 K for 6 h using aqueous solutions containing 2, 20, or 200 mM of $Al(NO_3)_3$. The most dominant spectral feature is the intense sharp peak observed at 3696.9 cm^{-1}, which is in good agreement with the XRD data in that pure $Mg(OH)_2$ has been reported to exhibit a single band at 3698 cm^{-1} due to the high basicity of its O—H groups [67]. The shoulder band at 781 cm^{-1} can be ascribed to the Al-OH translational mode [68], while the bands at 1370–1520 cm^{-1} are attributed to the symmetric and asymmetric stretching modes of CO_3^{2-} in the interlayer [69, 84]. The peak at approximately 1385 cm^{-1} is attributed to the ν_3 vibrational mode of NO_3^- with D_{3h} symmetry in the interlayer [46]. These peaks and bands were present in the spectra of all samples that had peaks attributable to Mg-Al LDH in the irrespective XRD patterns. An additional band at 1630–1650 cm^{-1} is assigned to the bending mode of water molecules in the interlayer, which are confirmed by

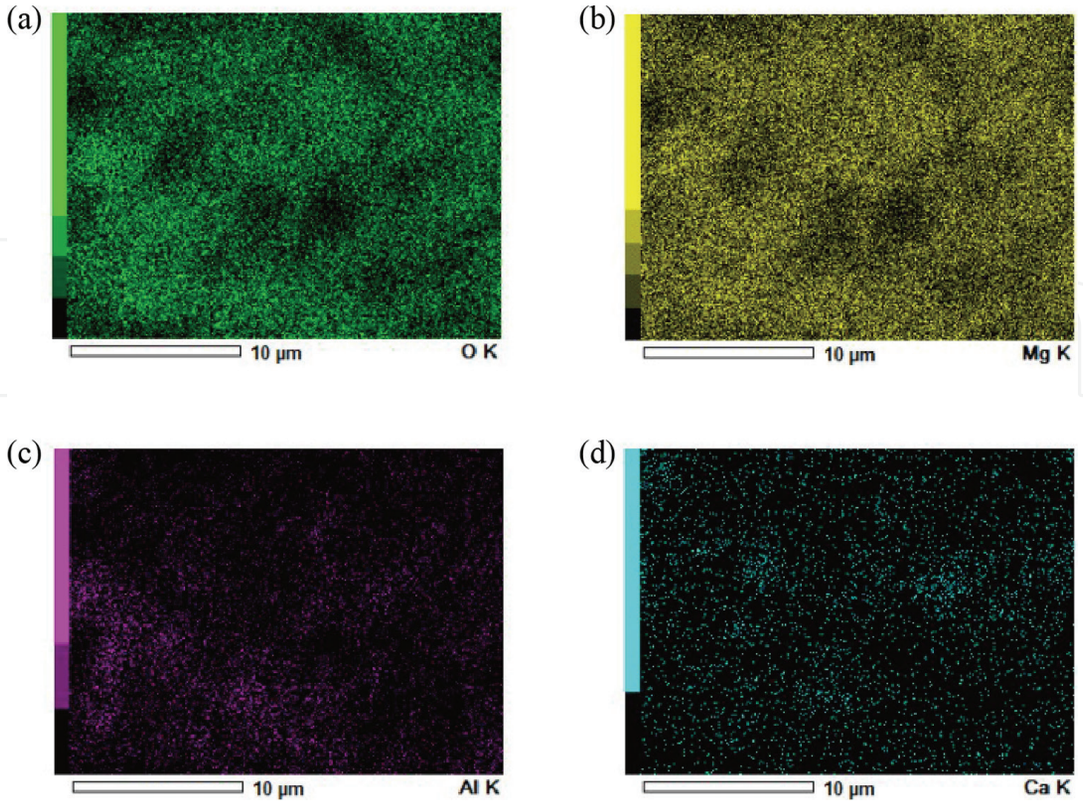

Figure 13. Elemental mapping images of AMCa602 Mg alloy after steam coating at 433 K for 6 h using an aqueous solution containing 20 mM $Al(NO_3)_3$: (a) O, (b) Mg, (c) Al, and (d) Ca [Corrosion Science, 2015, 92, 76–84, doi:10.1016/j.corsci.2014.11.031. Copyright @ELSEVIER (2015)].

the shoulder band at 3080 cm^{-1} and means that hydrogen bonding can occur between H_2O and carbonate ions in the interlayer [84]. These results demonstrate that all films were composed of crystalline $Mg(OH)_2$, nitrate-based Mg-Al LDH ($Mg_{1-x}Al_x(OH)_2(NO_3)_x \cdot nH_2O$), and carbonate-based Mg-Al LDH ($Mg_{1-x}Al_x(OH)_2(CO_3)_{x/2} \cdot nH_2O$).

Figure 15(a) presents a cross-sectional SEM image of the film prepared at 433 K for 6 h from an aqueous solution containing 200 mM of $Al(NO_3)_3$, which reveals that it had a thickness of about 197 μm. In comparison, the films prepared under the same conditions from 2 and 20 mM $Al(NO_3)_3$ solutions were estimated to be about 308 and 193 μm, respectively. All of the films formed from an aqueous solution containing $Al(NO_3)_3$ were much thicker than the 53 μm achieved with only H_2O, which implies that the existence of $Al(NO_3)_3$ in a closed autoclave accelerates film growth. The elemental mapping images in **Figure 5(b–d)** reveal that the films contained mostly Mg and O, implying that they were composed mainly of $Mg(OH)_2$. This result is in agreement well with the XRD profiles and FT-IR spectra obtained from each of the samples. A small trace of Al was also detected, demonstrating that Mg-Al LDH is presented locally in the film. Based on these XRD, FT-IR, and SEM-EDX results, it is concluded that steam coating is capable of forming $Mg(OH)_2$ and Mg-Al LDH on both AMCa602 and AZ31.

From the results presented in this section, the proposed mechanism by which films are formed by steam treatment can be described as follows. First, an aqueous solution containing

$Al(NO_3)_3$ is heated in the electric oven to generate steam containing Al^{3+} and NO_3^- ions that then saturates a closed reaction vessel. When this steam makes contact with the AMCa602 Mg alloy, the Mg metal it contains is readily dissolved into Mg^{2+} ions due to the high temperature and pressure. It is likely that $Mg(OH)_2$ crystallites are subsequently formed via a dissolution-precipitation mechanism, resulting in the formation of $Mg(OH)_2$ on the surface of the AMCa602 substrate. This is predicated on a notion by Nordlien et al. that amorphous platelets of $Mg(OH)_2$ are initially formed by the precipitation of Mg^{2+} or other soluble Mg species [70]. In addition, Mg^{2+}, Al^{3+}, and NO_3^- ions have the potential to react with the steam and form nitrate-based Mg-Al LDH. Any carbonate ions generated from CO_2 present in the enclosed autoclave atmosphere before steam treatment can result in the formation of carbonate-based Mg-Al LDH. Thus, along with $Mg(OH)_2$, both nitrate- and carbonate-based Mg-Al LDHs can form on AMCa602. Even if these reactions only occur at the surface, they can still progress at the interface between AMCa602, and the overlying film as the steam is able to penetrate thanks to the difference in pressure and its high kinetic energy. The end result is that a film composed of $Mg(OH)_2$ and Mg-Al LDH is directly formed on AMCa602. A porous film formed during the early stage of the process will allow more steam to pass through, resulting

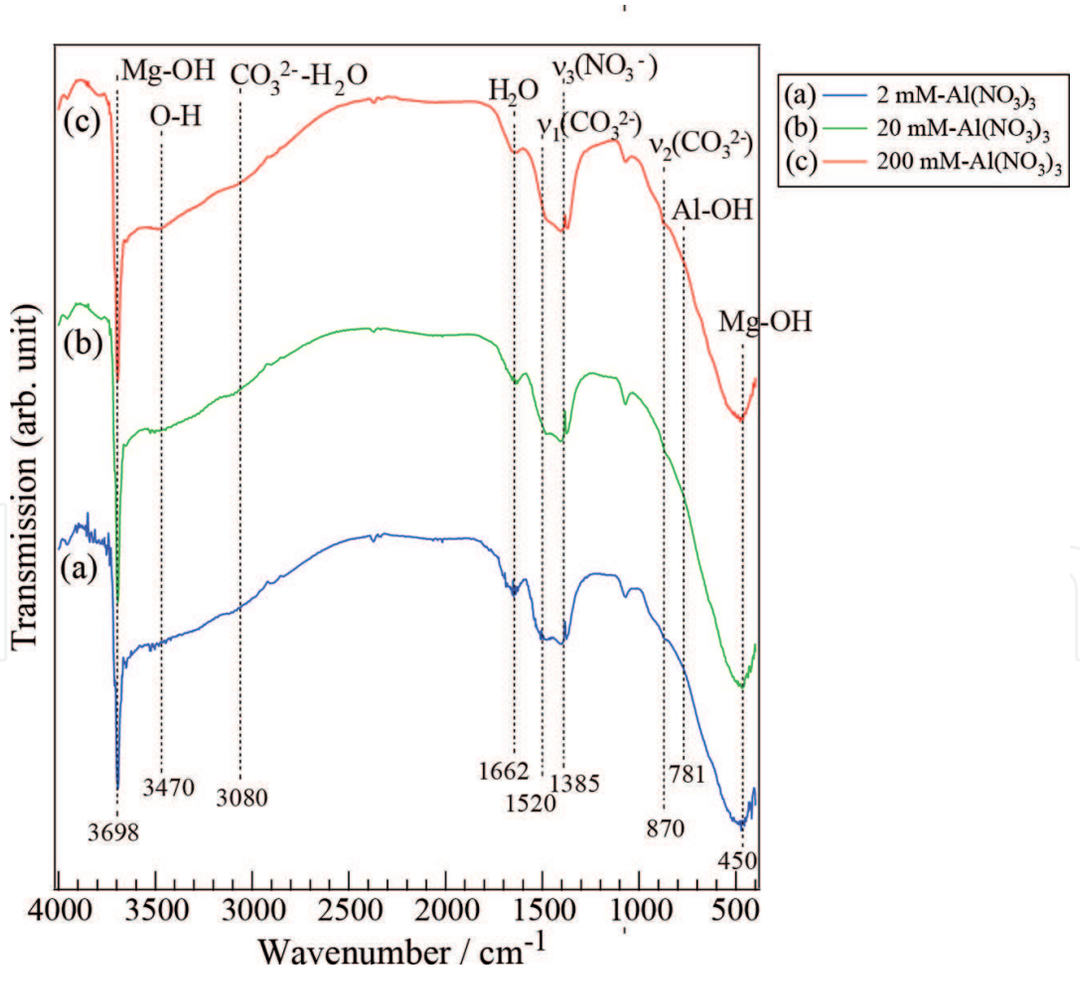

Figure 14. FT-IR spectra of AMCa602 Mg alloy after steam coating at 433 K for 6 h using aqueous solutions containing (a) 2, (b) 20, and (c) 200 mM of $Al(NO_3)_3$ [Corrosion Science, 2015, 92, 76–84, doi:10.1016/j.corsci.2014.11.031. Copyright @ELSEVIER (2015)].

http://dx.doi.org/10.5772/66365

in a thicker final film. In contrast, it is difficult for steam to easily penetrate a dense initial film. Thus, the film thickness is considered to be dependent on the preparation conditions.

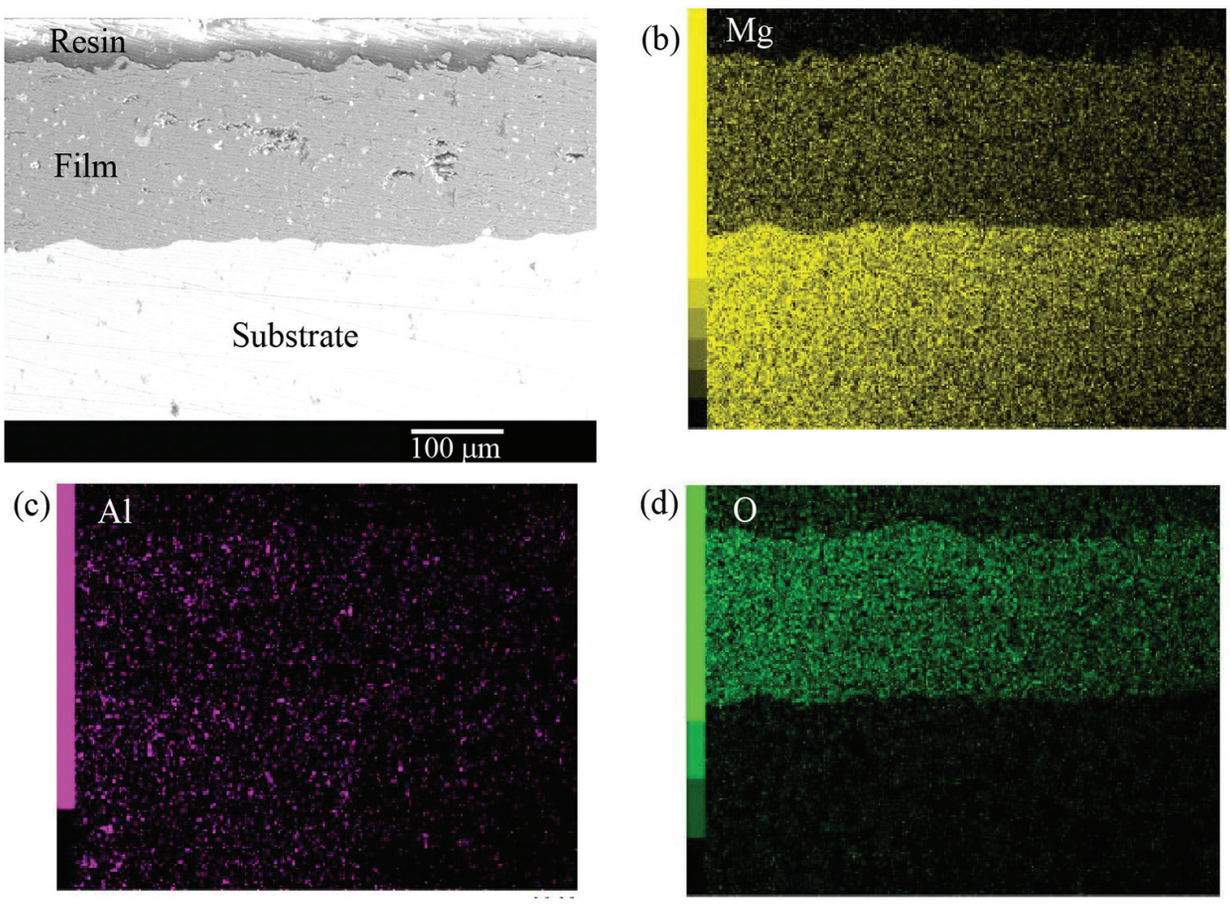

Figure 15. (a) Cross-sectional SEM image of the film prepared at 433 K for 6 h from an aqueous solution containing 200 mM $Al(NO_3)_3$ and elemental mapping images for (b) Mg, (c) Al, and (d) O [Corrosion Science, 2015, 92, 76–84, doi:10.1016/j.corsci.2014.11.031. Copyright @ELSEVIER (2015)].

The corrosion resistance of the film formed on the AMCa602 Mg alloy at 433 K for 6 h from aqueous solutions containing 0, 2, 20, and 200 mM $Al(NO_3)_3$ was estimated from the potentiodynamic polarization curves shown in **Figure 16**. For reference, the potentiodynamic polarization curve of untreated AMCa602 is shown in **Figure 6**. The corrosion potentials (E_{corr}) and corrosion current densities (j_{corr}) of the untreated AMCa602 and samples prepared under various conditions are listed in **Table 3** along with the Tafel slopes (β_a, anodic; β_c, cathodic) obtained from the polarization curve for each sample. The E_{corr} and j_{corr} values for the untreated AMCa602 were estimated to be −1.524 V vs. Ag/AgCl/sat.-KCl and 4.214×10^{-5} A cm^{-2}, respectively. In the cathodic region of the bare AMCa602, hydrogen evolution dominated at potentials that were more negative than E_{corr} (i.e., negative potentials with magnitudes above 1.524 V), resulting in an increase in the cathodic current density. The anodic region of the curve for the bare AMCa602 can be distinguished into two ranges. The first of these starts from E_{corr} (low anodic overpotential, −1.524 V) and is defined by an abrupt linear increase in the logarithm of

the current density, with a shift toward a positive voltage in the potential. It is in this region that dissolution reaction of Mg to Mg^{+} or Mg^{2+} ions is most likely to have occurred [71]. As the potential moved toward values more positive than −1.4 V vs. Ag/AgCl/sat.-KCl (i.e., negative potentials with magnitudes below 1.4 V and positive potentials), a current plateau occurred as a result of the electrode surface being covered with $Mg(OH)_2$ [72]. It has been reported that the anodic region of the polarization curves for AZ31 can be distinguished into three ranges [72],

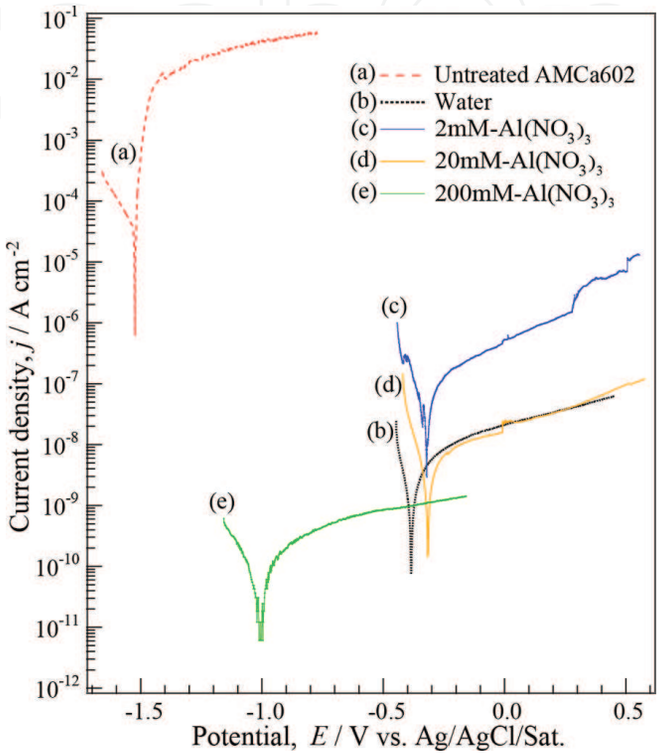

Figure 16. Potentiodynamic polarization curves of samples treated at 433 K for 6 h using aqueous solutions containing 0, 2, 20, and 200 mM of $Al(NO_3)_3$. The scanning rate was 0.5 mV s^{-1} [Corrosion Science, 2015, 92, 76–84, doi:10.1016/j.corsci.2014.11.031. Copyright @ELSEVIER (2015)].

which means that the overpotential for the dissolution of metallic magnesium to magnesium ions (Mg^{+} and/or Mg^{2+}) for AMCa602 is lower than that of AZ31. This improved dissolution might have resulted from the addition of Ca, as this is more reactive than Mg.

Figure 17 shows the potentiodynamic polarization curves for the bare AMCa602 and the samples that were treated at 433 K for 6 h from aqueous solutions containing 0, 2, 20, and 200 mM $Al(NO_3)_3$. Note that the current densities in the anodic and cathodic regions for all film-coated samples were lowered compared to the bare AMCa602 (**Figure 6**) and reproducibly low (**Figure 7**), demonstrating that all films improved the corrosion resistance of AMCa602. The E_{corr} also shifted toward a more positive value independent of the $Al(NO_3)_3$ concentration. At potentials more positive than E_{corr}, extended passive regions were clearly observed in the curves of the samples prepared from aqueous solutions containing 0 and 200 mM $Al(NO_3)_3$, as shown in **Figure 6**. These perfect passive regions imply that the film effectively protected AMCa602 in a solution containing Cl^{-} ions. The j_{corr} values decreased with an increase in the $Al(NO_3)_3$ concentration, and this was independent of the film thickness. Any increase in the

thickness and/or density of a film is generally beneficial to improving corrosion resistance by inhibiting contact between the metal surface and a corrosive solution. In this case, the film prepared from an aqueous solution containing 2 mM $Al(NO_3)_3$ was the thickest of all of the samples, and so this is expected to provide the best corrosion resistance. However, the

	E_{corr} (V vs. Ag/AgCl)	j_{corr} (A/cm^2)	Tafel slope (mV/decade)
Untreated AMCa602	−1.524	$4.21 \times 10^{-5} \pm 4.82 \times 10^{-5}$	b_a: 21.2 b_c: −178.7
Film coated AMCa602 prepared from ultrapure water	−0.385	$1.85 \times 10^{-9} \pm 9.85 \times 10^{-10}$	b_a: 198.7 b_c: −66.9
Film coated AMCa602 prepared from 2 mM $Al(NO_3)_3$	−0.322	$7.86 \times 10^{-8} \pm 7.68 \times 10^{-7}$	b_a: 278.1 b_c: −164.0
Film coated AMCa602 prepared from 20 mM $Al(NO_3)_3$	−0.316	$1.16 \times 10^{-9} \pm 2.39 \times 10^{-9}$	b_a: 235.4 b_c: −56.2
Film coated AMCa602 prepared from 200 mM $Al(NO_3)_3$	−1.007	$9.56 \times 10^{-11} \pm 2.17 \times 10^{-10}$	b_a: 288.6 b_c: −198.0

Table 3. Fitting results for potentiodynamic polarization curves in 5.0 wt.% NaCl solution for films formed using different concentrations of $Al(NO_3)_3$.

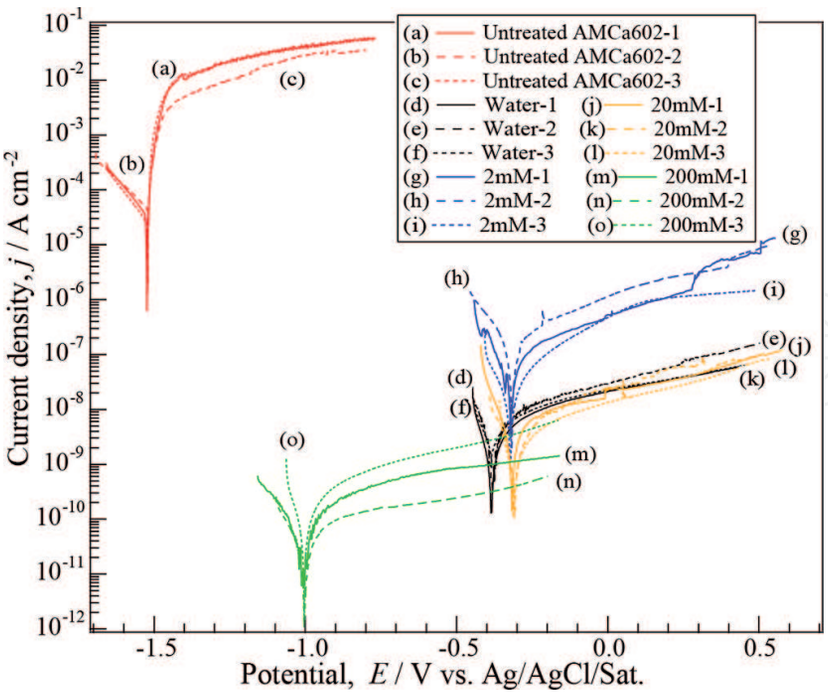

Figure 17. Potentiodynamic polarization curves for AMCa602 Mg alloy treated at 433 K for 6 h using aqueous solutions containing 0, 2, 20, and 200 mM of $Al(NO_3)_3$. Each system represents three repeat polarization curves (labeled 1, 2, and 3) measured under identical conditions to demonstrate reproducibility [Corrosion Science, 2015, 92, 76–84, doi:10.1016/j.corsci.2014.11.031. Copyright @ELSEVIER (2015)].

low density of this film produced the highest j_{corr} value, as explained earlier in the discussion regarding the formation mechanism. Thus, although the films prepared from aqueous solutions containing 20 and 200 mM $Al(NO_3)_3$ were of comparable thickness, their j_{corr} values suggest that they had very different densities.

An increase in current density at approximately 0.3 and 0 V vs. Ag/AgCl/sat.-KCl was observed in the polarization curves of the samples prepared from aqueous solutions containing 2 and 20 mM $Al(NO_3)_3$, which suggests that the corrosive solution permeated through cracks or pores in the film and initiated pitting corrosion. Similar behavior has been reported even in aluminum alloys [73], but in this case, the increase in current density was suppressed to produce a passive-like behavior with a shift in potential toward more positive values. This behavior suggests that the film might have some degree of self-healing functionality, which has been reported with Zn-Al LDH films formed on Al substrates that exhibited an increase in passive current density to initial values after immersion in a corrosive electrolyte [87]. In contrast, there is no evidence of pitting corrosion in the curve of the sample prepared from an aqueous solution containing 200 mM $Al(NO_3)_3$, which had E_{corr} and j_{corr} values estimated to be −1.007 V vs. Ag/AgCl/sat.-KCl and 9.560×10^{-11} A cm^{-2}, respectively, as shown in **Table 3**. This j_{corr} value was the lowest of all the samples, and as this is closely related to the rate of corrosion, this would suggest that a film prepared from 200 mM $Al(NO_3)_3$ offers the best corrosion resistance.

The correlations between the Mg-Al LDH content of the films, $Al(NO_3)_3$ concentration in solution, and corrosion current density are shown in **Figure 18**. The Mg-Al LDH content of the films was roughly estimated from the XRD peak intensity ratio of the (0 0 3) plane of Mg-Al LDH, $I_{LDH\text{-}003}$, to that of the (1 0 1) plane of $Mg(OH)_2$, $I_{Mg(OH)2\text{-}101}$, i.e., $I_{LDH\ content} = I_{LDH\text{-}003}/I_{Mg(OH)2\text{-}101}$. The peak intensities for these planes correspond to the strongest intensities in the standard powder diffraction data for $Mg(OH)_2$ and Mg-Al LDH. As the $Al(NO_3)_3$ concentration in the aqueous solution increased, the I_{LDH} content increased and the corrosion current density decreased, suggesting a strong relationship between the two. It has been reported that carbonate-based Mg-Al LDH shows anion exchangeability, whereby Cl^- ions are incorporated from NaCl solution and CO_3^{2-} ions are exhausted [51]. Moreover, nitrate-based Mg-Al LDH can abstract Cl^- by ejecting NO_3^- and so has an anion exchangeability that is higher than that of carbonate-based Mg-Al LDH. The Mg-Al LDH content of the films is therefore considered to have a significant effect on the corrosion current density, which is closely related to the rate of corrosion.

The durability of the corrosion-resistance performance of the sample prepared from an aqueous solutions containing 200 mM $Al(NO_3)_3$ was investigated by immersing it in a 5 wt.% NaCl solution. **Figure 19** shows the surface of the sample before immersion and after intervals of 5, 12, 24, 48, and 72 h. Note that the beige color of the film surface appeared to change slightly upon immersion, but no corrosion product or physical change in the appearance of the film was observed for up to 12 h. After 24 h of immersion, however, some spotty contrasts emerged that are likely the result of the film being damaged by the corrosive solution. An increase in the immersion time from 48 to 72 h led to a slight dissolution of the AMCa602 substrate at the corners of the sample, which is believed to be the progression of corrosion initiated by corrosive medium coming into contact with the substrate through a pit or minute pore in the film. Additionally, as corrosion resistance is known to be closely related to the film thickness, it is possible that the film

http://dx.doi.org/10.5772/66365

was simply thinner at the corner than at other points on the sample. This nonuniformity in film thickness could have occurred through differences in crystal growth at the edge of the substrate.

The SEM images in **Figure 20** show the sample surface before and after immersion in 5 wt.% NaCl solution for 24 and 72 h. It is evident from this that with an increase in immersion time, there was a change in the surface morphology and nanosheets that were slightly inclined with respect to the surface were more likely to be noticed on the surface. The EDX spectrum in **Figure 20(d)** revealed that there were two peaks attributable to Cl and Al at spot (i) in **Figure 20(c)**, but no evidence of a Na peak, which supports the earlier assertion that the Mg-Al LDH layer remained in the film and exhausted CO_3^{2-} and NO_3^- in exchange for Cl^- anions. Similarly, the absence of Cl and the presence of Al at spot (ii) also indicate that the Mg-Al LDH layer remained, which means that the nitrate or carbonate anions in the Mg-Al LDH layer were partially replaced with Cl^- anions.

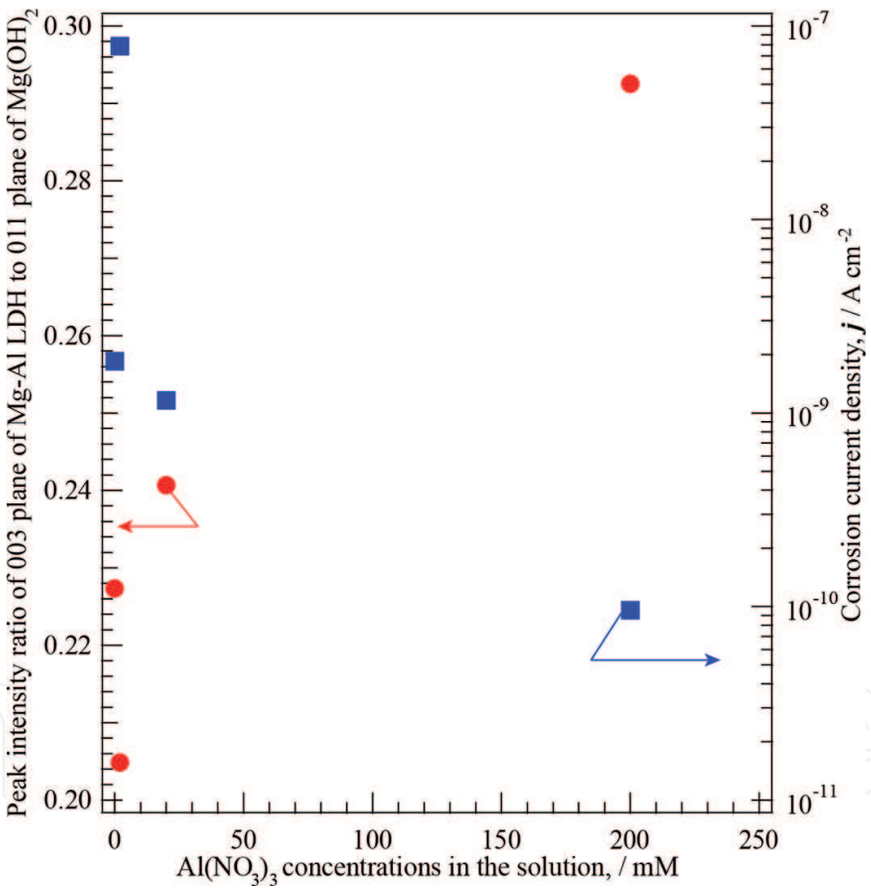

Figure 18. Correlation between Mg-Al LDH content of the film, $Al(NO_3)_3$ concentration in the aqueous solution, and corrosion current densities. The standard deviation of j_{corr} data for the samples obtained from aqueous solution containing 0, 2, 20, and 200 of mM $Al(NO_3)_3$ was 9.85×10^{-10}, 7.68×10^{-7}, 2.39×10^{-9}, and 2.17×10^{-10} A cm^{-2}, respectively [Corrosion Science, 2015, 92, 76–84, doi:10.1016/j.corsci.2014.11.031. Copyright @ELSEVIER (2015)].

Figure 21(a) presents XRD patterns obtained from the film-coated AMCa602 before and after immersion in 5 wt.% NaCl solution for 24 to 72 h. This shows that the peak attributable to the

(1 0 1) plane of the $Mg(OH)_2$ crystallite decreased slightly in intensity with an increase in immersion time, whereas that attributable to the (0 0 3) plane of the Mg-Al LDH crystallite increased in intensity. This indicates that even though the $Mg(OH)_2$ film was slightly dissolved in the corrosive solution, the Mg-Al LDH crystallite remained intact. The potentiodynamic polarization curves for the film-coated AMCa602 before and after immersion are shown in **Figure 21(b)**, from which the E_{corr} and j_{corr} values were determined to be −0.348 V vs. Ag/AgCl/sat.-KCl and 1.821×10^{-9} A cm^{-2}, respectively, after 24 h immersion, and −0.065 V vs. Ag/AgCl/sat.-KCl and 1.326×10^{-9} A cm^{-2} after 72 h. The E_{corr} shifted toward a more positive value with an increase in immersion time, which is possibly a result of the change in the ratio of anodic to cathodic sites on the surface that is caused by the dissolution of $Mg(OH)_2$ in the film. The j_{corr} value of the film-coated AMCa602 increased after immersion, indicating an increase in the corrosion rate that agrees well with the results of the immersion tests. This increase, however, was independent of the immersion time, with the j_{corr} value almost comparable after 24 and 72 h of immersion.

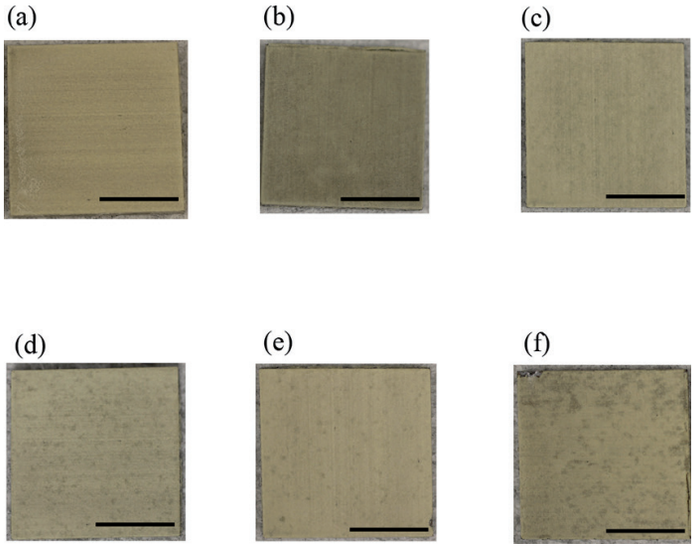

Figure 19. (a) Surface of AMCa602 Mg alloy after steam coating at 433 K for 6 h using an aqueous solution containing 200 mM $Al(NO_3)_3$ before immersion in a 5 wt.% NaCl aqueous solution. Same surface after immersion in a 5 wt.% NaCl aqueous solution for (b) 5, (c) 12, (d) 24, (e) 48, and (f) 72 h. All scale bars are 1 cm [Corrosion Science, 2015, 92, 76–84, doi:10.1016/j.corsci.2014.11.031. Copyright @ELSEVIER (2015)].

From the XRD patterns, SEM observations, EDX spectra, and polarization curve measurements, the mechanism by which a film produced by steam coating provides corrosion resistance to AMCa602 alloy can be explained as follows. At first, $Mg(OH)_2$ from the $Mg(OH)_2$/Mg-Al LDH composite film formed earlier on AMCa602 is dissolved to some extent through contact with a corrosive solution. This dissolution of $Mg(OH)_2$ causes the amount of Mg-Al LDH with anion exchangeability present on the film surface to increase gradually, leading to an increase in the intensity of the 0 0 3 reflection of Mg-Al LDH, as shown in **Figure 21(a)**. Due to the presence of Mg-Al LDH on the film surface, Cl^- ions can become trapped in the Mg-Al LDH, as shown in the EDS analysis, resulting in delaying corrosion. These results support the

http://dx.doi.org/10.5772/66365

hypothesis that the Mg-Al content of a $Mg(OH)_2$/Mg-Al LDH composite film is an key factor in improving the durability and corrosion resistance of the film. Moreover, steam coating produces a film that is thick and has a high density due to the presence of two phases of different sizes, namely, $Mg(OH)_2$ and Mg-Al LDH, which further contributes to improving the corrosion resistance of the film.

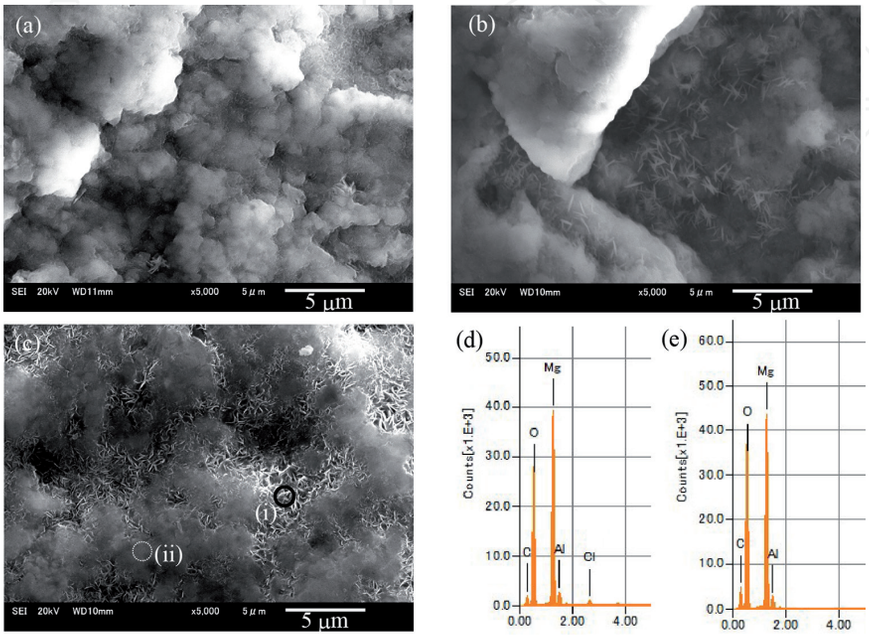

Figure 20. SEM images of sample surface (a) before and after immersion in 5 wt.% NaCl solution for (b) 24 and (c) 72 h. (d, e) EDX spectra obtained at spots (i) and (ii) in (c) [Corrosion Science, 2015, 92, 76–84, doi:10.1016/j.corsci.2014.11.031. Copyright @ELSEVIER (2015)].

In conclusion for this section, a film composed of $Mg(OH)_2$ and Mg-Al LDH was successfully formed on combustion-resistant AMCa602 Mg alloy by using an environmentally friendly steam coating method. Subsequent XRD and FT-IR studies confirmed that the film was composed of $Mg(OH)_2$ in combination with nitrate- and carbonate-based Mg-Al LDHs. The film thickness varied from 52 to 308 μm depending on the $Al(NO_3)_3$ concentration. A mechanism for the formation of such films was proposed based on the results of XRD, FT-IR, SEM, and EDX measurements, and the corrosion resistance was estimated by potentiodynamic measurements and immersion tests in 5 wt.% NaCl solution. A film prepared by steam coating at 433 K for 6 h using an aqueous solution of 200 mM $Al(NO_3)_3$ was found to have the highest corrosion resistance of all samples tested. The correlation between the Mg-Al LDH content of the film, $Al(NO_3)_3$, its corrosion current density, and the concentration of the aqueous solution used to create it was investigated, which revealed a strong correlation between the Mg-Al LDH content and corrosion current density. Based on the results achieved here with flame-resistant Mg alloy, we believe that our steam coating technique is an effective method for improving the corrosion resistance of both existing and future-generation Mg alloys.

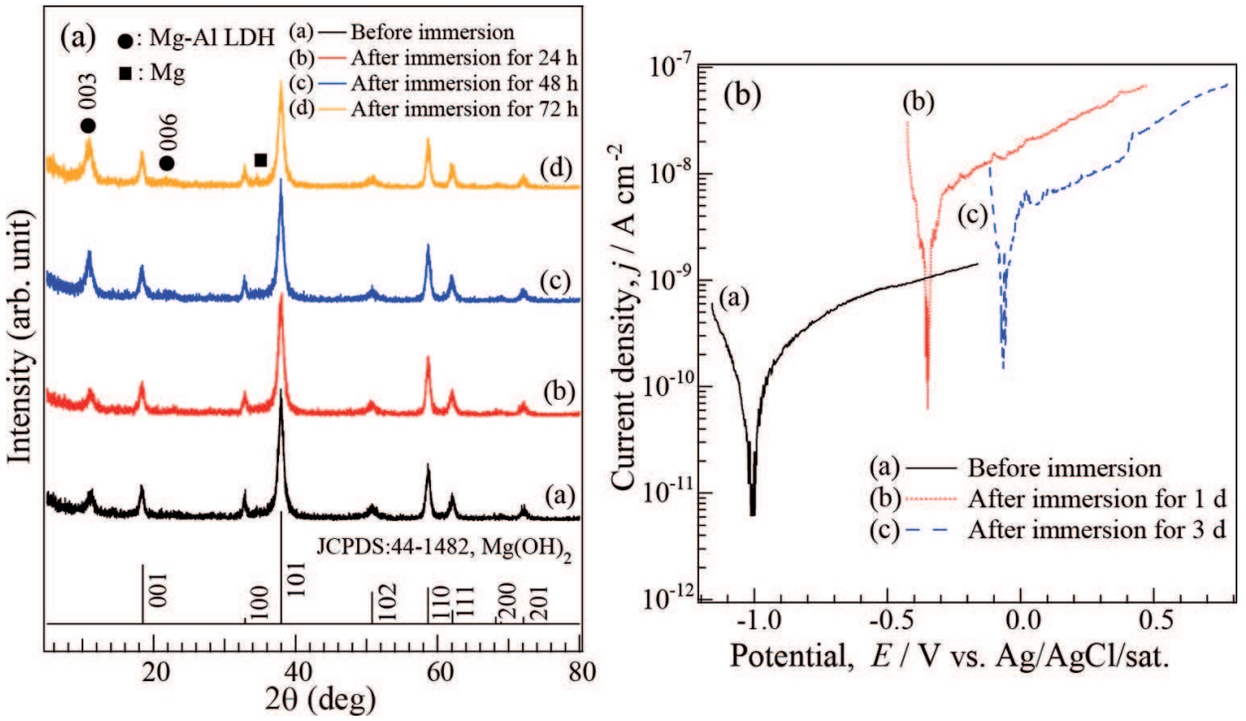

Figure 21. (a) GAXRD patterns and (b) potentiodynamic polarization curves of film-coated AMCa602 Mg alloy before and after immersion in 5 wt.% NaCl solution for 24 to 72 h [Corrosion Science, 2015, 92, 76–84, doi:10.1016/j.corsci.2014.11.031. Copyright @ELSEVIER (2015)].

4. Conclusion and outlook

This chapter has presented the results of experimental studies into the formation and corrosion resistance of an anticorrosive film composed of $Mg(OH)_2$ and Mg-Al LDH produced on AZ31 and AMCa602 Mg alloys by steam treatment. The physicochemical properties of the films were investigated using XRD, SEM, EDX, and FT-IR, and a mechanism for their formation was proposed based on these results. The corrosion resistance of the films produced on AZ31 and AMCa602 was estimated based on potentiodynamic measurements and immersion tests in 5 wt.% NaCl solution, which revealed that corrosion resistance of both alloys was improved by steam treatment. The Mg-Al LDH content of the films was also found to be strongly related to the corrosion current density. As Mg alloys are one of the more promising materials for reducing vehicle weight, thereby lowering fuel consumption and reducing CO_2 emission, any improvement in their inherently low corrosion resistance is of great value to increasing their wider-scale use. Thus, although there has already been a great deal of academic work and commercial interest in surface treatments for Mg alloys, we believe future work should focus on developing the steam coating process described here to greatly improve the corrosion resistance of a range of Mg alloys.

Acknowledgements

This research was partially supported by a grant for Advanced Industrial Technology Development from the New Energy and Industrial Technology Development Organization (NEDO) of Japan (no. 11B06024d), a grant-in-aid for young scientists (B) (no. 16 K18249) from the Japan Society for the Promotion of Science, and the Japan Science and Technology Agency (JST), Adaptable and Seamless Technology Transfer Program through Target-driven R&D (A-step: no. AS251Z02997K and AS2815047S).

Author details

Takahiro Ishizaki*[,1], Mika Tsunakawa[2], Ryota Shiratori[2], Kae Nakamura[2] and Ai Serizawa[1]

*Address all correspondence to: ishizaki@shibaura-it.ac.jp

1 Department of Materials Science and Engineering, College of Engineering, Shibaura Institute of Technology, Koto-ku, Japan

2 Department of Materials Science and Engineering, Graduate School of Engineering and Science, Shibaura Institute of Technology, Koto-ku, Japan

References

[1] Song G L, Atrens A, Quondam MX. Corrosion mechanisms of magnesium alloys. Advanced Engineering Materials. 1999; 1:1:11–33. DOI: 10.1002/(SICI)1527-2648(199909)1:1<11::AID-ADEM11>3.0.CO;2-N

[2] Shreir L L, editor. Corrosion Volume 1. London: Newnes-Butterworths; 1965. 86 p. ISBN: 0408001097

[3] Pokhmurska H, Wielage B, Lampke T, Grund T, Student M, Chervinska N, Quondam MX. Post-treatment of thermal spray coatings on magnesium. Surface and Coatings Technology. 2008; 202:18:4515–4524. DOI: 10.1016/j.surfcoat.2008.04.036

[4] Ghali E. Magnesium and magnesium alloys. In: Revie R W, editor. Uhlig's Corrosion Handbook. 3rd ed. New York: John Wiley & Sons; 2000, 793 p. DOI: 10.1002/9780470872864

[5] Pardo A, Merino M C, Coy A E, Arrabal R, Viejo F, Matykina E, Quondam MX. Corrosion behaviour of magnesium/aluminium alloys in 3.5 wt.% NaCl. Corrosion Science. 2008; 50:823–834. DOI: 10.1016/j.corsci.2007.11.005

[6] Liu Z, Gao W, Quondam MX. Electroless nickel plating on AZ91 Mg alloy substrate. Surface and Coatings Technology. 2006; 200:5087–5093. DOI: 10.1016/j.surfcoat.2005.05.023

[7] Lian J S, Li G Y, Niu L Y, Gu C D, Jiang Z H, Jiang Q, Quondam MX. Electroless Ni–P deposition plus zinc phosphate coating on AZ91D magnesium alloy. Surface and Coatings Technology. 2006; 200:5956–5962. DOI: 10.1016/j.surfcoat.2005.09.007

[8] Barchiche C E, Rocca E, Juers C, Hazan J, Steinmetz J. Corrosion resistance of plasma-anodized AZ91D magnesium alloy by electrochemical methods. Electrochimica Acta. 2007; 53:417–425. DOI: 10.1016/j.electacta.2007.04.030

[9] Montemor M F, Ferreira M G S, Quondam MX. Electrochemical study of modified bis-[triethoxysilylpropyl] tetrasulfide silane films applied on the AZ31 Mg alloy. Electrochimica Acta. 2007; 52:7486–7495. DOI: 10.1016/j.electacta.2006.12.086

[10] Zhang D, Gou Y, Liu Y, Guo X, Quondam MX. A composite anodizing coating containing superfine Al_2O_3 particles on AZ31 magnesium alloy. Surface and Coatings Technology. 2013; 236:52–57. DOI: 10.1016/j.surfcoat.2013.04.059

[11] Guo X, Du K, Guo Q, Wang Y, Wang F, Quondam MX. Experimental study of corrosion protection of a three-layer film on AZ31B Mg alloy. Corrosion Science. 2012; 65:367–375. DOI: 10.1016/j.corsci.2012.08.055

[12] Hamdy A S, Doench I, Mohwald H, Quondam MX. Smart self-healing anti-corrosion vanadia coating for magnesium alloys. Progress in Organic Coatings. 2011; 72:387–393. DOI: 10.1016/j.porgcoat.2011.05.011

[13] Gigandet M P, Faucheu J, Tachez M, Quondam MX. Formation of black chromate conversion coatings on pure and zinc alloy electrolytic deposits: role of the main constituents. Surface and Coatings Technology. 1997; 89:3:285–291. DOI: 10.1016/S0257-8972(96)03013-7

[14] Anandan C, William Grips V K, Rajam K S, Jayaram V, Bera P, Quondam MX. Investigation of surface composition of electrodeposited black chrome coatings by X-ray photoelectron spectroscopy. Applied Surface Science. 2002; 191:254–260. DOI: 10.1016/S0169-4332(02)00192-7

[15] Bayati M R, Shariat M H, Janghorban K, Quondam MX. Design of chemical composition and optimum working conditions for trivalent black chromium electroplating bath used for solar thermal collectors. Renewable Energy. 2005; 30:2163–2178. DOI: 10.1016/j.renene.2005.02.003

[16] Budavari S, O'Neil M, Smith A, Heckelman P, Obenchain J. The Merck Index: An Encyclopedia of a Chemical, Drugs and Biologicals. 12th ed. Boca Raton: CRC Press; 1996. 1475 p. ISBN: 0911910123

[17] Elsentriecy H H, Azumi K, Konno H, Quondam MX. Effect of surface pretreatment by acid pickling on the density of stannate conversion coatings formed on AZ91 D magnesium alloy. Surface and Coatings Technology. 2007; 202:532–537. DOI: 10.1016/j.surfcoat.2007.06.033

[18] Chong K Z, Shih T S, Quondam MX. Conversion-coating treatment for magnesium alloys by a permanganate–phosphate solution. Materials Chemistry and Physics. 2003; 80:191–200. DOI: 10.1016/S0254-0584(02)00481-9

[19] Rudd A L, Breslin C B, Mansfeld F, Quondam MX. The corrosion protection afforded by rare earth conversion coatings applied to magnesium. Corrosion Science. 2000; 42:275–288. DOI: 10.1016/S0010-938X(99)00076-1

[20] Takenaka T, Ono T, Narazaki Y, Naka Y, Kawakami M, Quondam MX. Improvement of corrosion resistance of magnesium metal by rare earth elements. Electrochimica Acta. 2007; 53: 117–121. DOI: 10.1016/j.electacta.2007.03.027

[21] Zucchi F, Frignani A, Grassi V, Trabanelli G, Monticelli C, Quondam MX. Stannate and permanganate conversion coatings on AZ31 magnesium alloy. Corrosion Science. 2007; 49:4542–4552. DOI: 10.1016/j.corsci.2007.04.011

[22] Scholes F H, Soste C, Hughes A E, Hardin S G, Curtis P R, Quondam MX. The role of hydrogen peroxide in the deposition of cerium-based conversion coatings. Applied Surface Science. 2006; 253:1770–1780. DOI: 10.1016/j.apsusc.2006.03.010

[23] Yang L, Li J, Lin C, Zhang M, Wu J, Quondam MX. Study of molybdenum/lanthanum-based composite conversion coatings on AZ31 magnesium alloy. Applied Surface Science. 2011; 257:2838–2842. DOI: 10.1016/j.apsusc.2010.10.077

[24] Zeng R, Lan Z, Kong L, Huang Y, Cui H, Quondam MX. Characterization of calcium-modified zinc phosphate conversion coatings and their influences on corrosion resistance of AZ31 alloy. Surface and Coatings Technology. 2011; 205:3347–3355. DOI: 10.1016/j.surfcoat.2010.11.027

[25] Khaselev O, Yahalom J, Quondam MX. Constant voltage anodizing of Mg-Al Alloys in KOH-$Al(OH)_3$ solutions. Journal of The Electrochemical Society. 1998; 145:190–193. DOI: 10.1149/1.1838234

[26] Yerokhin A L, Nie X, Matthews L A, Dowey S J, Quondam MX. Plasma electrolysis for surface engineering. Surface and Coatings Technology. 1999; 122:73–93. DOI: 10.1016/S0257-8972(99)00441-7

[27] Kuhn A, Quondam MX. Plasma anodizing of magnesium alloys. Metal Finishing. 2003; 101:44–50. DOI: 10.1016/S0026-0576(03)90261-3

[28] Ma Y, Nie X, Northwood D O, Hu H, Quondam MX. Systematic study of the electrolytic plasma oxidation process on a Mg alloy for corrosion protection. Thin Solid Films. 2006; 494:296–301. DOI: 10.1016/j.tsf.2005.08.156

[29] Luo H, Cai Q, He J, Wei B, Quondam MX. Preparation and properties of composite ceramic coating containing Al_2O_3-ZrO_2-Y_2O_3 on AZ91D magnesium alloy by plasma electrolytic oxidation. Current Applied Physics. 2009; 9:1341–1346. DOI: 10.1016/j.cap.2009.02.017

[30] Li X, Liu X Y, Luan B L, Quondam MX. Corrosion and wear properties of PEO coatings formed on AM60B alloy in $NaAlO_2$ electrolytes. Applied Surface Science. 2011; 257:9135–9141. DOI: 10.1016/j.apsusc.2011.05.115

[31] Hussein R O, Zhang P, Nie X, Xia T, Northwood D O, Quondam MX. The effect of current mode and discharge type on the corrosion resistance of plasma electrolytic oxidation (PEO) coated magnesium alloy AJ62. Surface and Coatings Technology. 2011; 206:1990–1997. DOI: 10.1016/j.surfcoat.2011.08.060

[32] Birss V, Xia S, Yue R, Richard G R Jr, Quondam MX. Characterization of oxide films formed on Mg-based WE43 alloy using AC/DC anodization in silicate solutions. Journal of the Electrochemical Society. 2004; 151:B1–10. DOI: 10.1149/1.1629095

[33] Wang Y, Wang J, Zhang J, Zhang Z, Quondam MX. Characteristics of anodic coatings oxidized to different voltage on AZ91D Mg alloy by micro-arc oxidization technique. Materials and Corrosion. 2005; 56:88–92. DOI: 10.1002/maco.200403822

[34] Hsiao H Y, Tsung H C, Tsai W T, Quondam MX. Anodization of AZ91D magnesium alloy in silicate-containing electrolytes. Surface and Coatings Technology. 2005; 199:127–134. DOI: 10.1016/j.surfcoat.2004.12.010

[35] Blawert C, Heitmann V, Dietzel W, Nykyforchyn H M, Klapkiv M D, Quondam MX. Influence of process parameters on the corrosion properties of electrolytic conversion plasma coated magnesium alloys. Surface and Coatings Technology. 2005; 200:68–72. DOI: 10.1016/j.surfcoat.2005.02.035

[36] Srinivasan P B, Liang J, Blawert C, Störmer M, Dietzel W, Quondam MX. Effect of current density on the microstructure and corrosion behaviour of plasma electrolytic oxidation treated AM50 magnesium alloy. Applied Surface Science. 2009; 255:4212–4218. DOI: 10.1016/j.apsusc.2008.11.008

[37] Sreekanth D, Rameshbabu N, Venkateswarlu K, Quondam MX. Effect of various additives on morphology and corrosion behavior of ceramic coatings developed on AZ31 magnesium alloy by plasma electrolytic oxidation. Ceramics International. 2012; 38:4607–4615. DOI: 10.1016/j.ceramint.2012.02.040

[38] Stojadinović S, Vasilić R, Petković M, Belča I, Kasalica B, Perić M, Zeković L J, Quondam MX. Luminescence during anodization of magnesium alloy AZ31. Electrochimica Acta. 2012; 59:354–359. DOI: 10.1016/j.electacta.2011.10.084

[39] Khaseleva O, Weiss D, Yahalom J, Quondam MX. Anodizing of pure magnesium in KOH-aluminate solutions under sparking. Journal of the Electrochemical Society. 1999; 146:1757–1761. DOI: 10.1149/1.1391838

[40] Bonilla F A, Berkani A, Liu Y, Skeldon P, Thompson G E, Habazaki H, Shimizu K, John C, Stevens K, Quondam MX. Formation of anodic films on magnesium alloys in an alka-

line phosphate electrolyte. Journal of The Electrochemical Society. 2002; 149:B4–B13. DOI: 10.1149/1.1424896

[41] Ghasemi A, Raja V S, Blawert C, Dietzel W, Kainer K U, Quondam MX. Study of the structure and corrosion behavior of PEO coatings on AM50 magnesium alloy by electrochemical impedance spectroscopy. Surface and Coatings Technology. 2008; 202:3513–3518. DOI: 10.1016/j.surfcoat.2007.12.033

[42] Arrbal R, Matykina E, Viejo F, Skeldon P, Thompson G E, Quondam MX. Corrosion resistance of WE43 and AZ91D magnesium alloys with phosphate PEO coatings. Corrosion Science. 2008; 50:1744–1752. DOI: 10.1016/j.corsci.2008.03.002

[43] Liang J, Srinivasan P B, Blawert C, Dietzel W, Quondam MX. Influence of pH on the deterioration of plasma electrolytic oxidation coated AM50 magnesium alloy in NaCl solutions. Corrosion Science. 2010; 52:540–547. DOI: 10.1016/j.corsci.2009.10.011

[44] Srinivasan P B, Liang J, Balajeee R G, Blawert C, Stormer M, Dietzel W, Quondam MX. Effect of pulse frequency on the microstructure, phase composition and corrosion performance of a phosphate-based plasma electrolytic oxidation coated AM50 magnesium alloy. Applied Surface Science. 2010; 256:3928–3935. DOI: 10.1016/j.apsusc.2010.01.052

[45] Yagi S, Sengoku A, Kubota K, Matsubara E, Quondam MX. Surface modification of ACM522 magnesium alloy by plasma electrolytic oxidation in phosphate electrolyte. Corrosion Science. 2012; 57:74–80. DOI: 10.1016/j.corsci.2011.12.032

[46] Collazo A, Hernández M, Nóvoa X R, Pérez C, Quondam MX. Effect of the addition of thermally activated hydrotalcite on the protective features of sol–gel coatings applied on AA2024 aluminium alloys. Electrochimica Acta. 2011; 56:7805–7814. DOI: 10.1016/j.electacta.2011.03.067

[47] Lin J K, Uan J Y, Quondam MX. Formation of Mg,Al-hydrotalcite conversion coating on Mg alloy in aqueous HCO_3^-/CO_3^{2-} and corresponding protection against corrosion by the coating. Corrosion Science. 2009; 51:1181–1188. DOI: 10.1016/j.corsci.2009.02.007

[48] Chen J, Song Y, Shan D, Han E H, Quondam MX. In situ growth of Mg–Al hydrotalcite conversion film on AZ31 magnesium alloy. Corrosion Science. 2011; 10:3281–3288. DOI: 10.1016/j.corsci.2011.06.0033

[49] Lin J K, Jeng K L, Uan J Y, Quondam MX. Crystallization of a chemical conversion layer that forms on AZ91D magnesium alloy in carbonic acid. Corrosion Science. 2011; 53:3832–3839. DOI: 10.1016/j.corsci.2011.07.035

[50] Chen J, Song Y, Shan D, Han E H, Quondam MX. Study of the in situ growth mechanism of Mg–Al hydrotalcite conversion film on AZ31 magnesium alloy. Corrosion Science. 2012; 33:148–158. DOI: 10.1016/j.corsci.2012.05.022

[51] Cavani F, Trifirò F, Vaccari A, Quondam MX. Hydrotalcite-type anionic clays: preparation, properties and applications. Catalysis Today. 1991; 11:2:173–301. DOI: 10.1016/0920-5861(91)80068-K

[52] Poznyak S K, Tedim J, Rodrigues L M, Salak A N, Zheludkevich M L, Dick L F P, Ferreira M G S, Quondam MX. Novel inorganic host layered double hydroxides intercalated with guest organic inhibitors for anticorrosion applications. ACS Applied Materials & Interfaces. 2009; 1:10:2353–2362. DOI: 10.1021/am900495r

[53] Zheludkevich M L, Poznyak S K, Rodrigues L M, Raps D, Hack T, Dick L F, Nunes T, Ferreira M G S, Quondam MX. Active protection coatings with layered double hydroxide nanocontainers of corrosion inhibitor. Corrosion Science. 2010; 52:2:602–611. DOI: 10.1016/j.corsci.2009.10.020

[54] Buchheit R G, Guan H, Mahajanam S, Wong F, Quondam MX. Active corrosion protection and corrosion sensing in chromate-free organic coatings. Progress in Organic Coatings. 2003; 47:3–4:174–182. DOI: 10.1016/j.porgcoat.2003.08.003

[55] Tedim J, Poznyak S K, Kuznetsova A, Raps D, Hack T, Zheludkevich M L, Ferreira M G S, Quondam MX. Enhancement of active corrosion protection via combination of inhibitor-loaded nanocontainers. ACS Applied Materials & Interfaces. 2010; 2:5:1528–1535. DOI: 10.1021/am100174teira

[56] Tedim J, Zheludkevich M L, Salak A N, Lisenkov A, Ferreira M G S, Quondam MX. Nanostructured LDH-container layer with active protection functionality. Journal of Materials Chemistry. 2011; 21:15464–15470. DOI: 10.1039/C1JM12463C

[57] Montemor M F, Snihirova D V, Taryba M G, Lamaka S V, Kartsonakis I A, Balaskas A C, Kordas G C, Tedim J, Kuznetsova A, Zheludkevich M L, Ferreira M G S, Quondam MX. Evaluation of self-healing ability in protective coatings modified with combinations of layered double hydroxides and cerium molibdate nanocontainers filled with corrosion inhibitors. Electrochimica Acta. 2012; 60: 31–40. DOI: 10.1016/j.electacta.2011.10.078

[58] Lin J K, Hsia C L, Uan J Y, Quondam MX. Characterization of Mg, Al-hydrotalcite conversion film on Mg alloy and Cl^- and CO_3^{2-} anion-exchangeability of the film in a corrosive environment. Scripta Materialia. 2007; 56:11:927–930. DOI: 10.1016/j.scriptamat.2007.02.020

[59] Tedim J, Kuznetsova A, Salak A N, Montemor M F, Snihirova D, Pilz M, Heludkevich M L, Ferreira M G S, Quondam MX. Zn-Al layered double hydroxides as chloride nanotraps in active protective coatings. Corrosion Science. 2012; 55:1–4. DOI: 10.1016/j.corsci.2011.10.003

[60] Wu G, Zeng X, Ding W, Guo X, Yao S, Quondam MX. Characterization of ceramic PVD thin films on AZ31 magnesium alloys. Applied Surface Science 2006; 252:7422–7429. DOI: 10.1016/j.apsusc.2005.08.095

[61] Kuo Y L, Chang K H, Quondam MX. Atmospheric pressure plasma enhanced chemical vapor deposition of SiO_x films for improved corrosion resistant properties of AZ31 magnesium alloys. Surface and Coatings Technology. 2015; 283:194–200. DOI: 10.1016/j.surfcoat.2015.11.004

[62] Wang J, Li D, Liu Q, Yin X, Zhang Y, Jing X, Zhang M, Quondam MX. Fabrication of hydrophobic surface with hierarchical structure on Mg alloy and its corrosion resistance. Electrochimica Acta. 2010; 55:6897–6906. DOI: 10.1016/j.electacta.2010.05.070

[63] Lom T S, Ryu H S, Hong S H, Quondam MX. Electrochemical corrosion properties of CeO_2-containing coatings on AZ31 magnesium alloys prepared by plasma electrolytic oxidation. Corrosion Science. 2012; 62:104–111. DOI: 10.1016/j.corsci.2012.04.043

[64] Ryu H S, Park D S, Hong S H, Quondam MX. Improved corrosion protection of AZ31 magnesium alloy through plasma electrolytic oxidation and aerosol deposition duplex treatment. Surface and Coatings Technology. 2013; 219:82–87. DOI: 10.1016/j.surfcoat.2013.01.008

[65] Zhang F, Sun M, Xu S, Zhao L, Zhang B, Quondam MX. Fabrication of oriented layered double hydroxide films by spin coating and their use in corrosion protection. Chemical Engineering Journal. 2008; 141:362–367. DOI: 10.1016/j.cej.2008.03.016

[66] Ishizaki T, Cho S P, Saito N, Quondam MX. Morphological control of vertically self-aligned nanosheets formed on magnesium alloy by surfactant-free hydrothermal synthesis. CrystEngComm. 2009; 11:2338–2343. DOI: 10.1039/B907490B

[67] Xu Z P, Zeng H C, Quondam MX. In-situ generation of maximum trivalent cobalt in synthesis of hydrotalcite-like compounds $Mg_xCoII_{1-x-y}CoIII_y(OH)_2(NO_3)_y{\cdot}nH_2O$. Chemistry of Materials. 2000; 12:9:2597–2603. DOI: 10.1021/cm000053f

[68] Millange F, Walton R I, O'Hare D, Quondam MX. Time-resolved in situ X-ray diffraction study of the liquid-phase reconstruction of Mg–Al–carbonate hydrotalcite-like compounds. Journal of Materials Chemistry. 2000; 10:1713–1720. DOI: 10.1039/B002827O

[69] Regnier P, Lasaga A C, Berner R A, Han K W, Zilm O H, Quondam MX. Mechanism of CO_3^{2-} substitution in carbonate-fluorapatite: evidence from FTIR spectroscopy, 13C NMR, and quantum mechanical calculations. American Mineralogist. 1994; 79:9–10:809–818.

[70] Nordlien J S, Ono S, Masuko N, Nisancioglu K, Quondam MX. A TEM investigation of naturally formed oxide films on pure magnesium. Corrosion Science. 1997; 39:8:1397–1414. DOI: 10.1016/S0010-938X(97)00037-1

[71] Tanaka D K, Long G G, Kruger J. Structure of the passive films on cast and rapidly solidified Mg alloys. In: Proceedings of 11th International Corrosion Congress; 2-9, April, 1990; Florence. London: The International Corrosion Council. 1990. 605–610.

[72] Baril G, Galicia G, Deslouis C, Pébère N, Tribollet B, Vivier V, Quondam MX. An impedance investigation of the mechanism of pure magnesium corrosion in sodium sulfate

solutions corrosion, passivation, and anodic films. Journal of the Electrochemical Society. 2007; 154:2:C108–C113. DOI: 10.1149/1.2401056

[73] Bobby Kannan M, Raja V S, Quondam MX. Influence of heat treatment and scandium addition on the electrochemical corrosion behavior of Al-Zn-Mg-Cu-Zr (7010) alloy. Metallurgical and Materials Transactions A. 2007; 38A:2843–2852. DOI: 10.1007/s11661-007-9303-6.

[74] Williams G, McMurray H N, Quondam MX. Anion-exchange inhibition of filiform corrosion on organic coated AA2024-T3 aluminum alloy by hydrotalcite-like pigments. Electrochemical and Solid-State Letters. 2003; 6:B9–B11. DOI:10.1149/1.1539771

[75] Masaki K, Ochi Y, Kakiuchi T, Kurata K, Hirasawa T, Matsumura T, Takigawa Y, Higashi K, Quondam MX. Thermodynamic properties of selenium in Ag-Pb alloy and lead oxide phases at 1273 K. Materials Transactions. 2009; 50:5:1148–1151. DOI: 10.2320/matertrans.M2009021

[76] Zeng R C, Zhang F, Lan Z D, Cui H Z, Han E H, Quondam MX. Corrosion resistance of calcium-modified zinc phosphate conversion coatings on magnesium–aluminium alloys. Corrosion Science. 2014; 88:452–459. DOI: 10.1016/j.corsci.2014.08.007

[77] Yang H Y, Guo X W, Chen X B, Birbilis N, Quondam MX. A homogenisation pre-treatment for adherent and corrosion-resistant Ni electroplated coatings on Mg-alloy AZ91D. Corrosion Science. 2014; 79:41–49. DOI: 10.1016/j.corsci.2013.10.024

[78] Cui X J, Liu C H, Yang R S, Fu Q S, Lin X Z, Gong M, Quondam MX. Duplex-layered manganese phosphate conversion coating on AZ31 Mg alloy and its initial formation mechanism. Corrosion Science. 2013; 76:474–485. DOI: 10.1016/j.corsci.2013.07.024

[79] Wan T T, Liu Z X, Bu M Z, Wang P C, Quondam MX. Effect of surface pretreatment on corrosion resistance and bond strength of magnesium AZ31 alloy. Corrosion Science. 2013; 66:33–42. DOI: 10.1016/j.corsci.2012.08.051

[80] Zhang J, Kang Z, Quondam MX. Effect of different liquid–solid contact models on the corrosion resistance of superhydrophobic magnesium surfaces. Corrosion Science. 2014; 87:452–459. DOI: 10.1016/j.corsci.2014.07.010

[81] Ivanou D K, Starykevich M, Lisenkov A D, Zheludkevich M L, Xue H B, Lamaka S V, Ferreira M G S, Quondam MX. Plasma anodized ZE41 magnesium alloy sealed with hybrid epoxy-silane coating. Corrosion Science. 2013; 73:300–308. DOI: 10.1016/j.corsci.2013.04.019

[82] Xia Y H, Zhang B P, Lu C X, Geng L, Quondam MX. Improving the corrosion resistance of Mg–4.0Zn–0.2Ca alloy by micro-arc oxidation. Materials Science and Engineering C, 2013; 33:5044–5050. DOI: 10.1016/j.msec.2013.08.033

[83] Mori Y, Koshi A, Liao J, Quondam MX. Corrosion resistance of plasma electrolytic oxidation layer of a non-ignitable Mg–Al–Mn–Ca magnesium alloy. Corrosion Science. 2016; 104:207–216. DOI: 10.1016/j.corsci.2015.12.013

[84] Xu Z P, Zeng H C, Quondam MX. Abrupt structural transformation in hydrotalcite-like compounds $Mg_{1-x}Al_x(OH)_2(NO_3)_x \cdot nH_2O$ as a continuous function of nitrate anions. The Journal of Physical Chemistry B. 2001; 105:9:1743–1749. DOI: 10.1021/jp0029257

[85] Rives V, Ulibarri M A, Quondam MX. Layered double hydroxides (LDH) intercalated with metal coordination compounds and oxometalates. Coordination Chemistry Reviews. 1999; 181:1:61–120. DOI: 10.1016/S0010-8545(98)00216-1

[86] Kuma K, Paplawsky W, Gedulin B, Arrhenius G, Quondam MX. Mixed-valence hydroxides as bioorganic host minerals. Origins of Life and Evolution of the Biosphere. 1989; 19:6:573–602. DOI: 10.1007/BF01808119

[87] Yan T, Xu S, Peng Q, Zhao L, Lei X, Zhang F, Quondam MX. Self-healing of layered double hydroxide film by dissolution/recrystallization for corrosion protection of aluminum. Journal of the Electrochemical Society. 2013; 160:10:C480–C486. DOI: 10.1149/2.053310jes

IntechOpen